Provenance information recorded by mineral inclusions in detrital garnet

Jan Schönig[1*], Guido Meinhold[1,2], Hilmar von Eynatten[1], Nils K. Lünsdorf[1]

[1]Department of Sedimentology and Environmental Geology, Geoscience Center Göttingen, University of Göttingen, Goldschmidtstraße 3, 37077 Göttingen, Germany

[2]School of Geography, Geology and the Environment, Keele University, Keele, Staffordshire, ST5 5BG, UK

[*]Correspondence should be addressed to J.S. (e-mail: jan.schoenig@uni-goettingen.de)

Abstract

Garnet single-grain analysis is an often used and well established tool in sedimentary provenance studies, especially when metamorphic source rocks are involved. So far, however, solely the geochemical composition of detrital garnets is considered to draw conclusions concerning probable source rocks. The gained information is often limited by (i) geochemical overlap of garnets derived from different lithology and metamorphic grade, (ii) similar probabilities of belonging to more than one source rock type, and (iii) the limitations of discriminating different protolith compositions. Here we present the first attempt of using mineral inclusions in detrital garnet as a provenance tool. We analyzed the inclusions of ~300 fine to medium sand-sized detrital garnets from two proximal modern sand samples taken in the HP/UHP Western Gneiss Region of SW Norway. All mineral inclusions ≥2 μm were identified by Raman spectroscopy, showing that (i) most garnets from HP/UHP metamorphic source rocks contain mineral inclusions ≥2 μm, (ii) Raman spectroscopy is a very powerful tool to characterize the inclusion types, and (iii) less stable mineral phases like kyanite, omphacite, diopside, enstatite, coesite, amphibole group, and epidote group minerals occur as inclusions in garnet. These minerals, which are important for provenance studies, can thus be preserved in the sedimentary record as long as garnet is stable. The combination of inclusion types in garnet and geochemical garnet classification shows that (i) inclusions well reflect the geological characteristics of the sampled catchments, implying that they are useful indicators for HP/UHP provenance, and (ii) inclusions in garnet can be used to support and enhance the provenance information obtained by garnet geochemistry.

Keywords: Sediment provenance; Garnet; Mineral inclusions; Raman spectroscopy; Western Gneiss Region

1. Introduction

Provenance studies often deal with changes in the source area arising from the temporal geodynamic evolution of the region.

In particular, the initiation of high-pressure (HP) and ultrahigh-pressure (UHP) metamorphic rocks as a sedimentary source is of specific interest, displaying the exposure of deep crustal levels in the source area, which typically has significant geologic and geodynamic implications. Characteristic HP/UHP metamorphic index minerals like glaucophane, lawsonite, omphacite, kyanite, or coesite are either mechanically and/or geochemically unstable. Therefore, these minerals progressively disappear when subjected to processes of the sedimentary cycle, and thus important provenance information gets lost. Additionally, HP/UHP rocks are often overprinted under lower-grade metamorphic conditions of the amphibolite and granulite facies during exhumation, whereby HP/UHP phases get usually replaced by lower-pressure phases. This leads to the fact that the mineral assemblages typically reflect retrograde stages, whereas the prograde and peak metamorphic history is obscured. Consequently, the transfer of characteristic HP/UHP index minerals into the sedimentary system may be hampered.

In contrast, information about prograde and peak metamorphic stages can be recorded and preserved in garnet, a heavy mineral which can grow during multiple metamorphic stages. Garnet is a very abundant metamorphic mineral covering a broad range of pressure–temperature (*P*–*T*) conditions and protolith compositions (e.g., Krippner et al., 2014). Because garnet composition is a function of these parameters, and garnet is comparatively stable during surface weathering, transport, and deep burial conditions (e.g., Morton and Hallsworth, 1999), several geochemical discrimination schemes have been developed and applied as a tool in sedimentary provenance analysis (see Krippner et al., 2014, for a review and evaluation). A recently published discrimination scheme by Tolosana-Delgado et al. (2017) operates with a multivariate statistical model to assign garnet grains with a certain probability to major host rock groups. Until now, however, all garnet provenance tools solely consider geochemical and isotopic garnet composition. Although it is well known from crystalline rocks that metamorphic garnet usually contains inclusions and that the occurrence and distribution of these inclusions can be used to deduce the metamorphic history of a rock (e.g., Thompson et al., 1977; Krogh, 1982; Faryad et al., 2010), this concept has not yet been thoroughly applied in provenance studies.

Here we present the distribution of mineral inclusions in detrital garnets from two proximal modern sand samples taken in the HP/UHP Western Gneiss Region of SW Norway. All mineral inclusions ≥2 µm of ~300 garnets (i.e., ~150 per sample) in the grain-size range 63–500 µm were identified by Raman spectroscopy. This technique has the advantages of (i) not being restricted to a specific sample preparation, allowing straightforward combination with other analytical techniques like the electron microprobe, (ii) being contact-free and having an excellent volume resolution due to the usage of a confocal microscope system adapted for the Raman spectrometer, enabling the identification of even small inclusions within the entire garnet volume, (iii) getting structural and implicitly geochemical information in a single step, so that even polymorphs like quartz and coesite can be distinguished, and (iv) being comparatively quick, which is important when analyzing a large number of garnet grains and mineral inclusions (e.g., Nasdala et al., 2004; Andò and Garzanti, 2014; Neuville et al., 2014). We compared the obtained inclusion data with the geochemical composition of the host garnets and show that (i) less stable but for provenance studies important mineral phases occur as inclusions in garnet, suggesting that these can be preserved in the sedimentary record as long as garnet is stable, (ii) inclusions in garnet well reflect the geological characteristics of the sampled catchments, implying that they are useful indicators for HP/UHP provenance, and (iii) inclusions in garnet can be used to support and enhance the provenance information given by geochemical garnet composition.

2. Geological setting

The two studied areas (Flatraket and Runde) are located in the Western Gneiss Region of SW Norway, which extends over an area of ~50,000 km^2 (Wain, 1997) between Bergen in the South and Trondheim in the North (Fig. 1). The Western Gneiss Region is composed of the autochthonous Western Gneiss Complex, overlain by a series of allochthonous Caledonian thrust nappes (Hacker et al., 2010). It is believed that the Western Gneiss Complex represents the westward continuation of the Baltic basement. Thus, the Western Gneiss Region is a large tectonic window through the allochthonous nappe pile, in which the Western Gneiss Complex is exposed as a large segment of the former craton Baltica (Roberts and Gee, 1985; Krabbendam and Wain, 1997; Beyer et al., 2012).

The Western Gneiss Complex mainly consists of orthogneisses, which were initially generated during the Gothian Orogeny (~1.7 to 1.5 Ga) and subsequently overprinted during the Sveconorwegian Orogeny (~1.3 to 0.9 Ga) (e.g., Beyer et al., 2012). The resulting metamorphic conditions ranged between amphibolite and granulite facies (Bingen et al., 2001; Røhr et al., 2004). Relicts of this event are rare and comprise ~1% of the Western Gneiss Complex (Wain et al., 2001; Peterman et al., 2009).

The Caledonian Orogeny in Paleozoic times is commonly subdivided into the pre-Scandian (not recognized in the Western Gneiss Complex; Hacker et al., 2010), the Scandian, and the post-Scandian metamorphic phases. The single phases can chronologically overlap and coexist in the broad area of the Western Gneiss Region.

The Scandian phase encompasses the time interval between early Silurian and early Devonian times (~435 to 400 Ma). During this phase, the two continental blocks Laurentia (western block) and Baltica (eastern block) collided under oblique plate convergence and final closure of the Iapetus Ocean (e.g., Roberts and Gee, 1985; Spengler et al., 2009; Hacker et al., 2010). This was accompanied by overthrusting and arrangement of the allochthonous nappes (e.g., Roberts and Gee, 1985; Andersen et al., 1990), forming the ~1000 km-long mountain system called the Scandinavian Caledonides (Beyer et al., 2012). The progressive convergence led to the subduction of Baltica's western continental margin beneath Laurentia (e.g., Torsvik and Cocks, 2005) and coherent HP/UHP metamorphism (e.g., Smith, 1984; Carswell and Cuthbert, 2003). The metamorphic grade and depth of subduction increased from SE towards the NW, as well as the intensity of deformation (e.g., Hacker et al., 2010). Temperature conditions ranged between ~550°C in the SE (Krogh, 1977; Griffin et al., 1985; Carswell and Cuthbert, 2003) and 850–950°C in the northernmost sector (Kylander-Clark et al., 2008). In the northernmost part also the highest pressure conditions were reached with up to 5.5–6.5 GPa (Scambelluri et al., 2008; Spengler et al., 2009), which were equalized to subduction depths of 180–200 km (van Roermund, 2009). Although the rocks were subjected to UHP conditions, they reacted only partially and locally (Corfu et al., 2014).

The post-Scandian metamorphic phase in Devonian times (~400 to 385 Ma) included the decompression and exhumation of the Western Gneiss Region to shallow crustal levels (e.g., Hacker et al., 2010). The exhumation was accomplished by coaxial E–W extension, vertical thinning, and minor N–S shortening. This led to a progressive exhumation of the Western Gneiss Region from SE to NW, which is contrary to the direction of the subduction during the Scandian phase (Krabbendam and Wain, 1997; Hacker et al., 2010; Spencer et al., 2013). Exhumation was accompanied by an extensive retrograde amphibolite to granulite facies metamorphic overprint with deformation and recrystallization (e.g., Krabbendam and Wain, 1997; Walsh and Hacker, 2004). This extensive and pervasive metamorphic overprint eliminated almost all records of HP/UHP metamorphism (e.g., Root et al., 2005). Solely dispersed eclogite bodies and eclogite facies rocks persisted (composing only ~1vol.% of the HP/UHP terrane) and record nearly all information about the HP/UHP metamorphism in the Western Gneiss Region (e.g., Wain et al., 2000).

The post-Scandian metamorphic phase was followed by a progressive exhumation of the UHP domains into the mid-upper crust by late folding, which continued through the late Devonian up to ~374 Ma (Hacker et al., 2010; Walsh et al., 2013). Today, three discrete UHP domains crop out within the Western Gneiss Region, which probably represent the cores of east-plunging antiforms. The distinct areas with UHP eclogites are separated by areas with HP eclogites (e.g., Root et al., 2005).

3. Sampling areas

The sampling area at Flatraket is located ~6 km north of the Nordfjord and ~17 km WSW of Åheim. The island of Runde is located ~55 km NW from Flatraket (Fig. 1). Both sampling areas are situated at the margins of an UHP domain, Flatraket at the western margin of the Nordfjord-Stadlandet UHP domain, and Runde at the western margin of the Sorøyana UHP domain (Root et al., 2005).

The stream-sediment sample at Flatraket (AK-N13-1: 61°58.554'N, 5°13.845'E) was taken a few meters upstream to the mouth of a northward draining stream so that mixing with sediments from coastal currents can be excluded (Krippner et al., 2016). In contrast, the sediment sample at Runde (AK-N37:

62°23.341'N, 5°38.252'E) represents a beach-sediment sample. However, because the sample was taken directly at the mouth of a small modern stream, and any morphological features indicating influences of coastal currents are absent, mixing with material transported along the shore can also be neglected for the sample from Runde (Schönig et al., 2018). Thus, the material in the two analyzed samples exclusively derived from the catchments marked by the watersheds in Fig. 1.

It is important to note that older sedimentary deposits could also be present in the catchments, which could scale up the area where the initial source rocks of the analyzed garnets might have been located (Schönig et al., 2018). In particular, glacial deposits in the Western Gneiss Region should be considered, which mainly originate from the Late Weichselian glaciation (Rye et al., 1987; Mangerud, 2004; Hughes et al., 2016). In the studied catchments, glacial deposits are thin but present (Goksøyr, 1938; Undås, 1942; Thoresen, 2013). However, even if the thin glacial deposits in the catchments could have provided small amounts of garnets to the sampled sediments, the ice flow direction coming exclusively from inland (e.g., Mangerud, 2004) only permit local sources within the Western Gneiss Region for the glacial deposits. Thus, the general HP/UHP signal from the Western Gneiss Region is not biased.

3.1 Flatraket

Within the catchment of the stream-sediment sample AK-N13-1, layered micaceous quartzo-feldspathic gneiss constitutes the major portion (Fig. 1). This gneiss was pervasively deformed during the post-Scandian phase of the Caledonian Orogeny, recrystallized under amphibolite facies conditions, and locally contains garnet (Krabbendam and Wain, 1997; Krabbendam et al., 2000). Eclogite pods <50 m in size are embedded in the micaceous gneiss. The cores of the pods are least affected by the amphibolite facies retrogression, and mafic bodies >10 m partially exhibit fresh eclogite within the core. The amphibolite facies overprint increases towards the pod margins and the outermost parts consist of amphibolite (Krabbendam et al., 2000). UHP metamorphism in this region is recorded by two known UHP eclogites, which contain bimineralic quartz/coesite inclusions in garnet and omphacite (Smith, 1984, 1985; Wain, 1997; Root et al., 2004; Smith and Godard, 2013; Schönig et al., 2018). However, both do not contribute material to the sediment sample AK-N13-1 because erosional material from the Flatraket harbor UHP eclogite (AK-N12) will be directly fed into the sea, and the UHP eclogite at Straumen is located outside the catchment in western direction (Fig. 1).

Besides the micaceous quartzo-feldspathic gneiss, the Flatraket complex is the next largest unit in the catchment, which consists of megacrystic felsic gneiss with a quartz-monzonitic composition and layered garnetiferous felsic gneiss, both showing also mafic parts (Krabbendam et al., 2000; Wain et al., 2001). In general, the complex represents a ~2 km^2 granulite facies low-strain enclave within the pervasively deformed and recrystallized amphibolite facies gneisses of the Western Gneiss Region (Wain, 1997; Wain et al., 2001). U–Pb ages of zircon and monazite indicate magmatic crystallization of the complex during the Gothian Orogeny at ~1680 to 1640 Ma and constrain timing of the granulite facies overprint to the Sveconorwegian Orogeny at ~1100 Ma (Corfu et al., 2014). During the Scandian phase of the Caledonian Orogeny, the majority of the complex remained dry and undeformed, whereby the Proterozoic granulite facies mineral assemblages preserved metastable. Eclogite facies rocks are restricted to zones of fluid infiltration and/or deformation and constitute ~5% of the complex (Wain et al., 2001; Corfu et al., 2014). During the subsequent post-Scandian metamorphic phase, the fluid infiltration was more extensive and leads to a pervasive amphibolite facies metamorphism on the retrograde part of the Caledonian orogenic cycle. More than 50% of the Flatraket Complex was affected by amphibolite facies hydration in different degrees, but granulite facies relicts are still present (Krabbendam et al., 2000; Wain et al., 2001). Several dykes and pods occur within the complex, including mafic to intermediate rocks (granulites, eclogites, locally retrogressed to amphibolite), dioritic to gabbroic rocks (primary granulite facies, strong amphibolite facies overprint, sometimes eclogitic assemblages at the rims, locally relictic magmatic texture in the core), and meta-anorthosites (mainly granulite facies).

Table 1 summarizes the mineralogical composition of the metamorphic rocks occurring in the sampled catchment of the stream-sediment sample AK-N13-1 and the close vicinity as outlined above. The heavy mineral spectra of the sample in the 63–125 µm grain-size fraction consists mainly of epidote group minerals and pyroxenes, followed by garnet, and much smaller amounts of amphibole group minerals, apatite, tourmaline, kyanite, olivine, rutile, and titanite (Krippner et al., 2016). In Fig. 1, also pebble samples (eclogites AK-N13-2a and AK-N13-2b and felsic gneisses AK-N13-2c and AK-N13-2d: 61°58.554'N, 5°13.845'E) and a crystalline rock sample (UHP eclogite AK-N12: 61°58.710'N, 5°14.063'E) from Krippner et al. (2016) were marked, which were used for geochemical comparison with the analyzed detrital garnets in this study.

3.2 Island of Runde

Within the catchment of the beach-sediment sample AK-N37, the largest unit is a micaceous quartzo-feldspathic orthogneiss (Fig. 1), which is also the main rock type of the whole region (northern Sorøyane). Its similarity to the common orthogneisses of the Western Gneiss Complex suggests an affiliation to the basement of Baltica (Root et al., 2005). Because of their similarity, the micaceous quartzo-feldspathic gneisses at Flatraket and Runde are not differentiated in Fig. 1, but note that the region around Runde experienced higher peak metamorphic temperatures (e.g., Kylander-Clark et al., 2008).

The next smallest rock unit on the island is a mylonitic quartzo-feldspathic gneiss, whereby only small divisions crop out at the outermost part of the sampled catchment. The mylonitic gneiss is locally garnetiferous (Krippner et al., 2016), contains amphibole (hornblende), and is of amphibolite facies. U–Pb ages in titanite ~384 Ma underline the pervasive retrogression during the post-Scandian phase (Spencer et al., 2013).

In the gneisses, numerous eclogite pods occur on the island of Runde, which – with a few exceptions – have not been mapped so far (Dahl, 1954; Root et al., 2004, 2005; Spencer et al., 2013; Krippner et al., 2016). Therefore, it can be assumed that various eclogite pods occur in the sampled catchment, although these are not shown in Fig. 1. For the shown eclogites, it is known that the eclogite at Langenes (AK-N38), ~1 km NE of the sampled catchment, contains garnet, sodic diopside (13% jadeite), magnesiohornblende, and rutile (Root et al., 2004). This eclogite is indicated as HP eclogite because no mineralogical evidence for UHP metamorphism is found so far, which might be related to the absence of silica. An adjacent silica-bearing eclogite a few hundred meters in the southern direction, in contrast, contains bimineralic coesite/quartz inclusions, displaying that the area underwent UHP conditions (Root et al., 2005). UHP metamorphism is also indicated by intact, monomineralic coesite inclusions found in detrital garnets of the same sample as studied here (AK-N37). Due to the geochemical variation of the detrital coesite-bearing host garnets and the variation in mineral inclusion assemblages, not only eclogites but also felsic rocks are considered as UHP source rocks (Schönig et al., 2018).

The heavy mineral spectra of the sample AK-N37 in the 63–125 µm grain-size fraction is dominated by pyroxenes and garnet, followed by significant amounts of amphibole group minerals, epidote group minerals, and apatite. Tourmaline, zircon, kyanite, olivine, rutile, and titanite occur in much smaller proportions (Krippner et al., 2016). In Fig. 1 also crystalline rock samples (eclogite AK-N38: 62°24.212'N, 5°39.230'E; and garnetiferous felsic gneiss AK-N39-1: 62°24.012'N, 5°39.459'E) from Krippner et al. (2016) were marked, which were used for geochemical comparison with the analyzed detrital garnets in this study.

4. Methods

4.1 Mineral separation and sample preparation

Mineral separation and sample preparation were performed at the University of Göttingen (Geosciences Center, Department of Sedimentology and Environmental Geology). About 300 g of both modern sand samples from Flatraket (AK-N13-1) and Runde (AK-N37) were wet-sieved to separate grain-size fractions, treated with acetic acid, split by quartering into amounts of 15–20 g, and the heavy mineral fraction was separated using sodium polytungstate with a density of 2.89 g cm^{-3}. Garnets were handpicked under the binocular microscope from three grain-size fractions (63–125 µm, 125–250 µm, 250–500 µm) and embedded in synthetic mounts using a bonding epoxy composed of a mixture of Araldite® resin and hardener at a ratio of 5:1. Mounts with the picked garnet crystals were ground with silicon carbide abrasive paper and polished in two steps with 3 µm and 1 µm Al_2O_3 abrasives in suspension. Overall ~350 grains per grain-size fraction and sample were picked (i.e., ~1050 per sample) and numbered in ascending order. For this study, the first 50 grains from each grain-size fraction were selected for inclusion analysis by Raman spectroscopy and geochemical analysis by the electron microprobe. This means grain numbers 1–50 (63–125 µm), 351–400 (125–250 µm), and 701–750 (250–500 µm) from sample AK-N13-1, and grain numbers 1–50 (63–125 µm), 351–400 (125–250 µm), and 706–755 (250–500 µm) from sample AK-N37.

4.2 Raman spectroscopy

Raman spectroscopy was performed at the University of Göttingen (Geosciences Center, Department of Sedimentology and Environmental Geology) using a Horiba Jobin Yvon XploRA Plus spectrometer equipped with an Olympus BX41 microscope, a 532 nm diode laser (25 mW maximum output power), and a motorized x-y-z stage. The confocal microscope is coupled to a 200 mm focal length spectrograph equipped with a four-grating turret (2400 l mm^{-1}, 1800 l mm^{-1}, 1200 l mm^{-1}, and 600 l mm^{-1}). All measurements were performed with maximum laser power, a confocal hole diameter and slit set to 100 µm, the 1800 l mm^{-1} grating, and a 100× objective with a numerical aperture of 0.9, where ~50% of the signal derive from an excitation volume depth of ~1.8 µm and ~95% derive from a volume depth of ~7.0 µm. For mineral identification of all inclusions ≥2 µm within the garnets, the spectrometer was calibrated on the 520.7 cm^{-1} line of Si, and the recorded spectrum was centered at 1000 cm^{-1}, covering a spectral field between ~100 cm^{-1} and ~1800 cm^{-1}.

Raman spectra of inclusions, in particular if they are small, are often masked by a strong signal from the garnet hosts. Therefore, most of the time the spectra of the garnet hosts were also captured directly next to the mineral inclusions to be identified, and subsequently the host spectra were subtracted from the inclusion/host mixed spectra, isolating the inclusion spectra (Fig. 2). In this way, sometimes inclusions <2 µm were also identified if they had a good Raman response (e.g., rutile), but only an identification of all inclusions ≥2 µm can be guaranteed. Captured spectra were exported to the software CrystalSleuth (Laetsch and Downs, 2006), the background was automatically subtracted via the software, and the corresponding mineral was identified by comparison with the RRUFF database (Lafuente et al., 2015) also via the CrystalSleuth software. For the obtained inclusion spectra in this study, mineral identification was made by comparison with the database and classification into inclusion types. Overall, all inclusions ≥2 µm in ~50 handpicked garnets from all three analyzed grain-size fractions were identified by Raman spectroscopy, i.e., ~150 garnets per sample and a total of ~300 garnets. For this, ~120 hours were spent in the Raman laboratory, which equates to ~2.5 garnets per hour.

4.3 Electron microprobe

Electron microprobe measurements were performed at the University of Göttingen (Geosciences Center, Department of Geochemistry) using a JEOL JXA 8900 RL electron microprobe equipped with five wavelength dispersive spectrometers. Before analysis, all samples were coated with carbon to ensure conductivity. Measurement conditions include an accelerating voltage of 15 kV and a beam current of 20 nA. Counting times were 15 s for Si, Mg, Ca, Fe, and Al, and 30 s for Ti, Cr, and Mn. The compositions of the ~50 detrital garnet grains from each of the three grain-size fractions (63–125 µm; 125–250 µm; 250–500 µm) were determined. Preferentially, the centers of the detrital grains were analyzed. Only when inclusions or fractures are located in the center, the measurement spot was shifted towards the rim.

5. Results

5.1 Mineral inclusions

5.1.1 Classification of inclusion types

By comparing the collected inclusion spectra with the database, a large number of mineral inclusions were identified. This includes oxides (coesite, corundum, quartz, rutile), feldspar group tectosilicates (albite, anorthoclase, labradorite, microcline, oligoclase, orthoclase, sanidine), mica group phyllosilicates (muscovite, phlogopite), pyroxene group (diopside, enstatite, omphacite) and amphibole group (actinolite, gedrite, tremolite) inosilicates, epidote group sorosilicates (clinozoisite, epidote, zoisite), nesosilicates (kyanite, zircon), the phosphate apatite, carbonate minerals (calcite, dolomite, magnesite, siderite), sulfate minerals (anhydrite, celestine, gypsum), and opaque minerals. The identification of specific mineral phases by simply comparing their Raman spectra with the database is sometimes unreliable, especially within individual mineral groups. However, the approach of using mineral inclusions identified by Raman spectroscopy as a metamorphic source rock indicator, as introduced here, should be straightforward without detailed analysis of every single spectrum. Therefore, the identification of the detected mineral phases by the RRUFF database was evaluated by validating specific spectral patterns. This results in a grouping of some phases into inclusion types to ensure their correct assignment and to focus on the most important information.

Due to their unique spectral Raman pattern, all detected oxides (coesite, corundum, quartz, rutile), nesosilicates (kyanite, zircon), and the phosphate apatite can be clearly identified and differentiated from other mineral phases (Fig. 3a–e), even if they are chemically similar and only differ in crystal structure like coesite and quartz (Fig. 3a). Therefore, all of them are indicated as single inclusion types, except corundum. Corundum was only found as small slices on the polished garnet surfaces of one garnet (<1%) from AK-N13-1 (Flatraket), and five garnets (~3%) from AK-N37 (Runde). Because Al_2O_3 (corundum) abrasives are used for polishing, these slices are considered to be contaminants and were thus excluded from further analysis.

Based on the Raman spectral pattern, feldspars can be readily identified by the presence of two or three peaks in the 450–515 cm^{-1} region, with the strongest peak between 505–515 cm^{-1} (Freeman et al., 2008). Several different members of the feldspar group tectosilicates were identified from the database as inclusions in the analyzed garnets. However, often similar high match probabilities are given for more than one member, in particular for the series orthoclase–sanidine–microcline and labrodorite–oligoclase–albite–anorthoclase, respectively. In this study, inclusions identified as orthoclase–sanidine–microcline were assigned to the alkali feldspar inclusion type, and inclusions identified as labrodorite–oligoclase–albite–anorthoclase to the plagioclase inclusion type. Alkali feldspar and plagioclase can be distinguished by the position of the strongest peak. For alkali feldspars this is located between 513–515 cm^{-1}, whereas all plagioclase main bands are located at <510 cm^{-1} (Mernagh, 1991; Freeman et al., 2008; Bersani et al., 2018). Because the tested inclusions which were assigned to the alkali feldspar type show the main band position of ≥ 514 cm^{-1} and those assigned to the plagioclase type ≤ 511 cm^{-1} (Fig. 3f), the classification of these two feldspar types based on the database seems reliable.

Phyllosilicates are easily distinguishable from the other major structural types of silicates. Within the group, however, the discrimination of specific types is more complicated, and the H_2O/OH spectral region (3500–3800 cm^{-1}) should be also considered (Wang et al., 2015). The phyllosilicate inclusion types identified by the database comprise the mica group minerals muscovite (also high match probabilities for trilithionite and paragonite) and phlogopite (also high match probabilities for fluorophlogopite). Collected spectra of both show a broad pattern in the 3500–3800 cm^{-1} region (Fig. 4), indicating the presence of H_2O, and thus, a complicated stacking sequence of tetrahedral and octahedral layers so that kaolinite–serpentine and pyrophyllite–talc group phyllosilicates can be excluded. The combined spectral pattern of the <1200 cm^{-1} and the 3500–3800 cm^{-1} region, in turn, makes an assignment to the mica group reliable. Furthermore, the strongest peak in the 600–800 cm^{-1} region of inclusions identified as muscovite by the database is located at >700 cm^{-1}, verifying an affiliation to the dioctahedral group of phyllosilicates like muscovite–paragonite. This is further supported by the presence of a peak at ~430 cm^{-1}, which is typical in Al-rich phyllosilicates. In contrast, the strongest peak in the 600–800 cm^{-1} region of inclusions identified as phlogopite by the database is located at <700 cm^{-1}, verifying an affiliation to the trioctahedral group of phyllosilicates like phlogopite–biotite. Furthermore the presence of a peak at ~350 cm^{-1} (present when Mg-rich), the absence of a peak at ~550 cm^{-1} (present when Fe-rich), and the position of the OH-bands between 3650–3750 cm^{-1} call for a more phlogopitic composition (spectrum evaluation based on Wang et al., 2015). However, because discrimination within the solid solution series is difficult and cannot be generalized, for this study, we assigned the mica group mineral inclusions to the muscovite–paragonite and phlogopite–biotite series, respectively.

Raman spectra of pyroxenes can be unambiguously distinguished from other minerals, and the spectral pattern also allows distinct discrimination between clinopyroxenes and orthopyroxenes, because clinopyroxenes have one intense band in the 650–700 cm^{-1} region (Fig. 5a), whereas orthopyroxenes show a doublet (Fig. 5b) (Mernagh and Hoatson, 1997; Wang et al., 2001; Buzatu and Buzgar, 2010).

In the analyzed garnet grains, some clinopyroxenes were identified as diopside by the database (sometimes also high match probabilities for augite), others as omphacite, and some give similar match probabilities for diopside and omphacite. In Fig. 5a, spectra of nine clinopyroxene inclusions are plotted in comparison with two diopside (ID 040009: $(Ca_{0.97}Fe_{0.02}Na_{0.01})_{\Sigma=1.00}(Mg_{0.97}Fe_{0.02}Al_{0.01})_{\Sigma=1.00}Si_{2.00}O_{6.00}$, ID 060171: $Ca_{1.00}$ $(Mg_{0.98}Mn_{0.02})_{\Sigma=1.00}Si_{2.00}O_{6.00}$) and one omphacite spectra (ID 061129.2: $(Ca_{0.51}Na_{0.48})_{\Sigma=0.99}$ $(Mg_{0.44}Al_{0.44}Fe^{2+}{}_{0.14}Fe^{3+}{}_{0.02})_{\Sigma=1.04}Si_{2.00}O_{6.00}$) from the RRUFF database, and one omphacite spectrum from the UHP eclogite exposed at Flatraket harbor (for location see Fig. 1). All spectra are ordered regarding the position of the main band, which ranges from ~665 cm^{-1} for the diopside spectra from the database to ~684 cm^{-1} for the spectrum of the omphacite inclusion in garnet grain number 702 of sample AK-N13-1 (Flatraket). The same trend can be observed for the bands of the triplet in the 300–420 cm^{-1} region, which positions continuously change from ~323 cm^{-1} (diopsides from database) to ~344 cm^{-1} (omphacite in grain number 702 of AK-N13-1) for the lowest frequency band, ~356 cm^{-1} to ~381 cm^{-1} for the intermediate band, and ~389 cm^{-1} to ~411 cm^{-1} for the highest frequency band.

Because all inclusions with high match probabilities for omphacite are located above the omphacite spectrum from the RRUFF database in Fig. 5a, and thus show higher Raman shifts for the Raman bands mentioned above, this inclusion type was classified as omphacite. Inclusions which show highest match probabilities for diopside or similar probabilities for diopside and omphacite, in contrast, are located below the omphacite spectrum but above the diopside spectra from the database. These inclusions were classified as diopside. Note that these diopsides may have variable amounts of an omphacite (jadeite) component which, however, cannot be quantified more precisely here.

Contrary to the clinopyroxenes, the orthopyroxenes give a clear picture, with all inclusion spectra giving the highest match probabilities for enstatite (example in Fig. 5b). Therefore, this inclusion type was classified as enstatite.

The identified amphiboles can be definitely assigned to the amphibole group, but discrimination within the group is not straightforward. Comparison with the database of different spectra from amphibole inclusions (Fig. 5c) gives similar high match probabilities for different amphibole group minerals like actinolite, gedrite, and tremolite. For a more precise discrimination the spectral region of H_2O/OH (3400–3800 cm^{-1}), spectra in different orientations from the same amphibole with polarized incident light (not appropriate for inclusions in mounted host mineral grains), and a reference amphibole with known chemistry should be considered (Leissner et al., 2015). This is not applicable in this study, and even if it was, uncertainties would remain due to high fluorescence, low signal-to-noise ratios, and possible impurities (Apopei and Buzgar, 2010). For these reasons, amphibole inclusions are classified as the amphibole group inclusion type, without any subdivision. The presence of glaucophane, however, can be excluded because the characteristic glaucophane band at ~385 cm^{-1} was not obtained in any of the amphibole group spectra.

Similar to the amphibole group inclusion type, also the epidote group minerals, the carbonate minerals, and the sulfate minerals were grouped. Epidote group mineral inclusions only occur in ~5% of the analyzed garnets in the Flatraket sample, and comparison with the database gives similar high match probabilities for clinozoisite, epidote, and zoisite, whereas in particular clinozoisite and epidote cannot be discriminated by their Raman spectra in the <1200 cm^{-1} region. Carbonate and sulfate minerals are more frequent in the samples and the database identified most of them as dolomites and anhydrites, respectively. However, in case of the carbonate minerals often high match probabilities are also given for magnesite, calcite and siderite. In the case of sulfate minerals, some inclusions are identified as gypsum and celestine, and others cannot be assigned to a specific sulfate mineral. Overall, the partially uncertain assignment to a specific mineral and the low significance of specific minerals of this group as a source rock indicator suggests that grouping as carbonate or sulfate minerals is sufficient for this study. Note, however, that most carbonate mineral inclusions are most likely dolomite and most sulfate mineral inclusions are most likely anhydrite.

Opaque minerals with a weak Raman response are present in ~5–7% of the analyzed garnets. They were not identified in this study and are excluded from further discussion. Identification requires long accumulation times and strong corrections to isolate the inclusion spectra from the inclusion/host mixed spectra, which is beyond the scope of this study.

Besides the mineral inclusions in the detrital garnets, CO_2 fluid inclusions were also detected. Fluid inclusions can provide information about different stages of rock formation, but fluid inclusion studies are very time consuming (van den Kerkhof and Hein, 2001) and are also beyond the scope of this study.

5.1.2 Inclusions in detrital garnets from Flatraket

Overall, 148 grains of the 150 analyzed grains (~99%) from the stream-sediment sample of Flatraket (AK-N13-1) are garnet. The two other mineral grains (grain number 15 = titanite; grain number 364 = enstatite) were confounded with garnet during picking. Of the 148 grains, 130 (~88%) exhibit inclusions which are sufficient in size (i.e., ≥2 µm) to be analyzed by Raman spectroscopy. The amount of garnets with analyzable inclusions increases with increasing grain size from ~84% (41 of 49) in the fine fraction (63–125 µm), over ~88% (43 of 49) in the medium fraction (125–250 µm), to ~92% (46 of 50) in the coarse fraction (250–500 µm). The detected inclusion types for each of the analyzed garnets from Flatraket are listed in Supplementary Table 1. In Supplementary Table 2 the proportion of the analyzed garnet grains with specific inclusion types is summarized. These results are shown in Fig. 6. In general, when inclusions of a specific type occur within the analyzed garnets, on average 1 to 4 inclusions of the same type are present in the garnet host. Only quartz inclusions are more frequent, with on average 5 to 20 inclusions per quartz-bearing garnet.

Quartz, rutile, and mica group minerals represent the main mineral inclusions, which are present in the bulk of the garnet grains. Quartz is the most frequent inclusion type, and is present in ~63% (82 of 130) of the garnets. The proportion of grains which exhibit quartz inclusions is almost constant over the three grain-size fractions (~61 to 65%). Rutile inclusions are also rather frequent and occur in ~43% (56 of 130) of the garnets. The coarser the grain-size fraction, the more frequent are rutile inclusions. Starting from ~29% of the garnet grains in the fine fraction, they are more frequent in the medium fraction (~44%), and the highest amount of rutile inclusions is found in the coarse fraction (~54%). Besides quartz and rutile, mica group minerals are abundant inclusions in garnet grains from Flatraket. They are composed of the muscovite–paragonite and phlogopite–biotite types. Phlogopite–biotite (~36%; 47 of 130) is more abundant than muscovite–paragonite (~23%; 30 of 130). Both together are present in ~52% (67 of 130) of the garnets. Generally, mica inclusions are more frequent in the fine grain-size fraction compared to medium and coarse fractions (Fig. 6).

The main mineral inclusions are followed by inclusions of apatite, sulfate minerals, and feldspars, which are present in a significant amount of the host garnets (~20 to 30%). Apatite inclusions occur in ~28% (37 of 130) of the garnet grains. While apatite inclusions in the fine fraction are only present in ~15% of the grains, they are more frequent in the medium and coarse fractions (~37% and ~33%, respectively). Inclusions of sulfate minerals are present in ~24% (31 of 130) of the garnets. Sulfate mineral inclusions are highest in the medium grain-size fraction with ~30%, and less abundant in the fine and coarse fraction (~20% and ~22%, respectively). Feldspar inclusions, including alkali feldspar and plagioclase, are present in ~22% (29 of 130) of the garnets. They are less frequent in the medium grain-size fraction with ~12%, but more abundant in the fine and coarse fractions (~24% and ~30%, respectively). The number of garnets with alkali feldspar inclusions is considerably smaller in the medium fraction (~2%) than in the fine (~15%) and coarse (~20%) fractions, while plagioclase inclusions are rather evenly distributed over all grain-size fractions (~9 to 13%; Fig. 6).

Carbonate minerals, clinopyroxenes, zircon, kyanite, epidote group minerals, and amphibole group minerals are less abundant and occur as inclusions in <20% of the garnets. Carbonates are present in ~12% (16 of 130) of the garnets. These are least frequent in the medium grain-size fraction (~7%) and more abundant in the fine and coarse fractions (~12% and ~17%, respectively). Overall, clinopyroxene inclusions are present in ~10% (13 of 130) of the garnets, with omphacite dominating over diopside (Fig. 6). While in the fine fraction only ~5% of the garnets contain inclusions of clinopyroxene, this number increases with increasing grains size to ~7% in the medium fraction and ~17% in the coarse fraction. Zircon and kyanite inclusions occur in ~7% (9 of 130) of the garnet grains. Both are most frequent in the coarse fraction (~15% and 13%, respectively), while in the two finer fractions they are rare (~2 to 5%). Inclusions of the epidote group and amphibole group minerals occur with ~5% (7 and 6 out of 130, respectively) of the garnets. Both are slightly more frequent in the fine fraction (~7%) and continuously decrease in the coarser fractions (Fig. 6).

5.1.3 Inclusions in detrital garnets from Runde

Overall, 150 grains (50 of every grain-size fraction) were analyzed from the beach-sediment sample of Runde (AK-N37), whereby 148 grains of it (~99%) are garnets, and two are other mineral grains which were confounded with garnet during picking (grain number 351 = plagioclase; grain number 395 = alkali feldspar). Of the 148 grains, 119 (~80%) exhibit inclusions ≥2 µm. The amount of garnet grains with inclusions ≥2 µm is almost constant and only slightly increases from ~78% (39 of 50) in the fine fraction (63–125 µm), over ~81% (39 of 48) in the medium fraction (125–250 µm), to ~82% (41 of 50) in the coarse fraction (250–500 µm). The detected inclusion types for each of the analyzed garnets from Runde are listed in Supplementary Table 3. In Supplementary Table 4 the proportion of the analyzed garnet grains with specific inclusion types is summarized. These results are shown in Fig. 7. In general, when inclusions of a specific type occur within the analyzed garnets, on average 1 to 4 inclusions of the same type are present in one garnet host. Only rutile inclusions are more frequent with on average 5 to 20 inclusions per rutile-bearing garnet.

The most frequent inclusion types within the garnets of the beach-sediment sample are quartz and rutile. Quartz inclusions are present in ~42% (50 of 119) of the grains. They are widespread in the medium grain-size fraction (~49%) and less frequent in the fine and coarse fractions (~38% and ~39%, respectively). Rutile inclusions occur in ~40% (48 of 119). They are also most common in the medium grain-size fraction (~51%) and less frequent in the coarse fraction (~44%). A much smaller amount (~26%) contain rutile inclusions in the fine grain-size fraction.

Inclusions of mica and feldspar group minerals are also present in significant amounts of the garnet grains. Mica group mineral inclusions are solely composed of phlogopite–biotite. They occur in ~24% (29 of 119) of the host garnets and show only minor fluctuations across the three grain-size fractions with a slight increase with increasing grain-size fraction (~23 to 27%). Feldspar inclusions are present in ~21% (25 of 119) of the garnets. They are composed of alkali feldspar and plagioclase inclusions, for which alkali feldspar is less frequent. Together, the amount of garnets which exhibit feldspar inclusions is almost constant over the three grain-size fractions (~20 to 23%). By considering alkali feldspar and plagioclase separately, an enrichment of both in the medium fraction compared to the fine and coarse fraction is indicated (Fig. 7).

Lower but also significant amounts of garnet grains carry inclusions of zircon, apatite, kyanite, and pyroxene. Zircon inclusions occur in ~18% (22 of 119) of the garnets. While the proportion of grains with zircon inclusions in the fine fraction is ~15%, and in the coarse fraction ~17%, they are slightly more frequent in the medium fraction where they were identified in ~23% of the garnets. Inclusions of apatite are present in ~18% (21 of 119) of the garnets. Both the fine and medium fraction, show ~15% grains with apatite inclusions. In the coarse fraction, apatite inclusions are more frequent and occur in ~22% of the grains. Kyanite inclusions are present in ~17% (20 of 119) of the studied garnet grains. With increasing grain-size fraction, the amount of garnets with kyanite inclusions increases from ~10 to 22%. Overall, ~15% (18 of 119) of the garnet grains exhibit pyroxene inclusions, whereas the amount decreases with increasing grain-size fraction. In the fine fraction, pyroxene inclusions occur in ~21%, in the medium fraction in ~13%, and in the coarse fraction in ~12% of the grains. Pyroxene inclusions include the two clinopyroxene types, omphacite and diopside, and the orthopyroxene type, enstatite. Clinopyroxene inclusions consist predominantly of diopside, which occurs in ~11% (13 of 119) of the garnets. Diopside is more frequent in the fine fraction

(~18%) than in the medium and coarse fraction (~8% and ~7%, respectively). Only 2 out of the 119 garnets (~2%) contain clinopyroxene inclusions which were classified as omphacite. Orthopyroxene (i.e., enstatite) inclusions are much less frequent than clinopyroxene inclusions. They are present in ~5% (6 of 119) of the garnets and in one-third of the cases the orthopyroxene inclusions are located in garnet grains which also carry clinopyroxene inclusions. With ~8%, the proportion of garnets that exhibit orthopyroxene inclusions is the highest in the medium grain-size fraction. In the coarse and fine fraction the proportion is lower (~5% and ~3%, respectively).

Furthermore, also carbonate mineral, amphibole group, and sulfate mineral inclusions are present in a smaller proportion of host garnets. Over the three grain-size fractions, carbonate mineral inclusions occur in ~9% (11 of 119) of the garnets. The amount of garnets with carbonate mineral inclusions decreases with increasing grain-size fraction (~18 to 5%). Amphibole inclusions occur in ~7% (8 of 119) of the grains. In the fine and medium fraction, ~8% of the garnets exhibit amphibole inclusions and in the coarse fraction they are slightly less frequent (~5%). Sulfate mineral inclusions occur in ~6% (7 of 119) of the garnets, and these are only present in the fine and medium fraction (~8% and ~10%, respectively).

In addition, three inclusions of coesite were identified in the analyzed grains. One in grain number 24 of the fine grain-size fraction and two in grain number 378 of the medium fraction. That means ~2% (2 of 119) of the analyzed garnet grains contain coesite inclusions. A detailed description of the coesite-bearing garnets, four more coesite-bearing garnets from the same sample, the characteristics of the coesite inclusions, and the resulting implications are given in Schönig et al. (2018).

5.2 Garnet geochemistry

The garnet compositions measured by the electron microprobe are given in Supplementary Table 5. Four garnet grains (grain number 22 from AK-N13-1, and grains 40, 395, and 732 from AK-N37) were excluded because the coating was damaged or the measured composition indicates contamination by inclusions. The compositions of the coesite-bearing garnets number 24 and 378 from sample AK-N37 (Runde) were measured at several spots (Schönig et al., 2018) and averaged for this study.

The multivariate statistical discrimination scheme of Tolosana-Delgado et al. (2017) was used to discriminate between garnet host rocks. Because the sampled catchments are almost exclusively composed of metamorphic rocks, we choose the prior probability ‘equal-M’ with equal probabilities of 30% for all metamorphic host-rock groups (A – eclogite facies; B – amphibolite facies; C – granulite facies), and significantly lower probabilities of 5% for ultramafic (D) and felsic plutonic rocks (E1). However, we also tested the prior probability ‘global’, and all analyzed garnets were still classified as metamorphic garnets.

Probabilities for the detrital host garnets of belonging to the major host-rock groups are given in Supplementary Table 5. These are plotted for the major metamorphic host-rock groups in Fig. 8a (Flatraket) and Fig. 9a (Runde). In Figs. 8b–i and 9b–i, these host-rock probabilities are shown separately for garnets with specific inclusion types. All of these ternary diagrams are complemented with pie charts indicating the proportion of grains belonging with highest probability to one of the metamorphic host-rock groups A, B, and C (for detailed numbers see Supplementary Table 6).

Overall, both catchments show similar characteristics. The major proportion of garnets (~59% for Flatraket, ~47% for Runde) show highest probability of belonging to the granulite facies group C, followed by garnets assigned to the eclogite facies group A (~39% and ~40%, respectively). Garnets assigned to the amphibolite facies group are subordinate (~3% and ~12%, respectively). This pattern is similar for all grain-size fractions, but garnets assigned to the amphibolite facies from the Flatraket sample are only present in the fine fraction.

Furthermore, quartz, rutile, kyanite, apatite, and zircon inclusions occur – with minimal deviation – in garnets of all geochemical compositions determined as the detrital overall composition (as illustrated in Figs. 8a, 9a). There are, however, variations in their proportions (see Supplementary Table 6 for exact proportions). Whereas kyanite inclusions in AK-N37 (Runde) show a similar distribution like the detrital overall composition (Fig. 9c), they are slightly less frequent in type A (eclogite facies) garnets of AK-N13-1 (Flatraket) (Fig. 8c). Quartz and apatite inclusions in both catchments are less frequent in type A garnets, but instead more abundant in type C (granulite facies) and/or type B (amphibolite facies) garnets (Figs. 8b, 8h, 9b, 9h). While rutile and zircon inclusions at Flatraket are more frequent in type A and less frequent in type C garnets (Figs. 8c, 8h), rutile inclusions are less frequent in type A garnets from Runde (Fig. 9c), and zircon inclusions from Runde show a similar pattern like the overall composition (Fig. 9h).

Inclusions of mica group minerals (muscovite–paragonite and phlogopite–biotite) and alkali feldspar are enriched in garnets of type C, and sometimes also type B, compared to type A garnets (Figs. 8f, 8g, 9f, 9g). In contrast, omphacite and epidote group inclusions are much more frequent in type A garnets, and do not occur, or only subordinated, in type B and C garnets (Figs. 8d, 8e, 9d). The same applies to diopside inclusions in the Flatraket sample (Fig. 8d), but in the sample from Runde diopsides are more abundant in type C garnets (Fig. 9d). However, these diopsides are mainly close to the transition zone between type A and C, and thus, have also high probabilities of belonging to type A. Enstatite and amphibole group inclusions show a very similar pattern to these diopside inclusions of the transition zone. They are more frequent in type C garnets, but the type C garnets often also have high probabilities of belonging to type A (Figs. 8e, 9d, 9e).

Inclusions of plagioclase, carbonate minerals, and sulfate minerals show a less distinct pattern. They are present in garnets of a large part of the overall composition, but not to the same extent like quartz, rutile, kyanite, apatite, and zircon. Plagioclase inclusions are slightly enriched in type A (Flatraket) or type B (Runde) garnets, compared to the overall composition (Figs. 8g, 9g). While inclusions of carbonate and sulfate minerals in the Flatraket sample are present in similar proportions of garnet types like the overall composition (Fig. 8i), carbonate mineral inclusions are more abundant in type C garnets and less abundant in type A garnets in the sample from Runde, which is contrary to the sulfate mineral inclusions in the Runde sample (Fig. 9i).

Coesite inclusions in the analyzed garnets from Runde are only present in type C garnets. However, this is an effect of the small number of garnets containing coesite. Schönig et al. (2018) analyzed an about five times larger number of garnets from the same sample and found six garnets with coesite inclusions, whereby three of the garnets are clearly classified as type C, one as type A, and two have almost equal probabilities of belonging to type A and C.

6. Discussion

6.1 Provenance information value of the obtained inclusion types

The high proportion (≥80%) of detrital garnet grains containing mineral inclusions ≥2 μm indicates that inclusions in garnets of metamorphic origin are potentially useful to gain provenance information. The ultimate aim is to identify specific metamorphic source rock types by analyzing these inclusions. When analyzing crystalline rocks, metamorphic facies types are differentiated by identification of diagnostic mineral assemblages, i.e., associations of mineral species in mutual grain contact (e.g., Bucher and Frey, 2002). In classical provenance studies, this information is not available due to the consideration of individual mineral grains which are not in contact with other mineral species. However, by considering mineral inclusions in the detrital single grains, mineral assemblage information of the source rocks can be obtained because the inclusions were entrapped during growth of the host mineral. Thus, an inclusion and its host mineral are coexisting since entrapment occurred during the same metamorphic stage. Caution should be taken when considering more than one inclusion in a single grain. Garnet, in particular, can record multiple metamorphic stages and isolate entrapped mineral inclusions from subsequent events. Thus, adjacent inclusions in garnet do not necessarily represent the same metamorphic stage. Therefore, mineral assemblages derived from more than one inclusion give hints but are no evidence for coexistence during entrapment. In contrast, when considering only single inclusions in garnet, these directly reflect a two-mineral assemblage (garnet host + inclusion phase), which coexisted during the same metamorphic stage (Schönig et al., 2018).

By focusing on diagnostic two-mineral assemblages, i.e., single mineral inclusions, the bulk of inclusion types detected in the analyzed garnets can be grouped regarding their use in source rock identification as (i) inclusions of little or no information, (ii) inclusions indicating a wide range of metamorphic source rocks, (iii) inclusions indicating a smaller range of metamorphic source rocks, and (iv) inclusions which yield specific source rock information.

(i) Quartz, feldspar, zircon, apatite, mica, carbonate minerals, and sulfate minerals are assigned to the group of **inclusions of little or no information**. Quartz and feldspars are abundant rock-forming minerals, which cannot be linked to a specific rock type. In general, quartz and alkali feldspar are more abundant in felsic lithologies, and plagioclase is more abundant in mafic lithologies, but all can also occur vice versa.

Especially eclogites often contain quartz. The presence of quartz inclusions also does not exclude pressure conditions of the coesite stability field during entrapment because quartz inclusions can be present very close to coesite inclusions, which – in some cases – is suggested to be a preservation effect of coesite inclusions (Schönig et al., 2018). Similar to quartz and alkali feldspar, apatite and zircon are also more frequent in felsic lithologies, but they occur in mafic rocks as well, so that they cannot be linked to a specific rock type. Likewise, also the mica group minerals, here muscovite–paragonite and phlogopite–biotite, carbonate and sulfate minerals, can occur in a wide range of metamorphic rocks, and do not point to specific *P*–*T* conditions during entrapment.

(ii) Amphibole group and epidote group inclusions are assigned to the group **indicating a wide range of metamorphic source rocks**. These hydrous minerals disappear at high temperatures in the granulite facies (Bucher and Frey, 2002). Thus, these inclusions cannot be captured by garnet growing during granulite facies conditions, and either temperature conditions have to be lower (e.g., amphibolite facies) or pressure conditions have to be higher (eclogite facies) during entrapment.

(iii) Kyanite, rutile, diopside, and enstatite are assigned to the group of **inclusions indicating a smaller range of metamorphic source rocks**. Kyanite belongs together with sillimanite and andalusite to the trimorphic Al_2SiO_5 group, which all together are only stable at the triple point at ~4.2 kbar and ~530°C (Bohlen et al., 1991). Due to their different stability fields, these aluminosilicates are often used as metamorphic index minerals, whereby the presence of kyanite is restricted to the HP parts of the greenschist, amphibolite, and granulite facies or even higher *P–T* ratios (Fig. 10a). Rutile is an abundant accessory mineral in medium- to high-grade metamorphic rocks (e.g., Force, 1980). It is newly formed at upper amphibolite facies conditions (or higher), and increasing pressure favors rutile formation (Zack et al., 2004). When subjected to lower-grade conditions at subsequent events, matrix rutile breaks down to form other titanium-bearing phases (Force, 1980; Zack et al., 2004). Therefore, it is very unlikely that garnet is able to capture rutile outside the *P–T* conditions where it is newly formed. Thus, a rutile inclusion in garnet reflects entrapment at upper amphibolite facies conditions or higher. Similarly, diopside inclusions also indicate upper amphibolite facies conditions or higher because diopside typically occurs in mafic to ultramafic rocks, in which the appearance of clinopyroxene defines the lower-grade boundary of the upper amphibolite facies (Bucher and Frey, 2002). The suggested omphacite component of the diopsides in this study, furthermore, point to even higher-grade metamorphic conditions. Enstatite is a typical orthopyroxene of high-temperature (HT) metamorphic rocks like granulites, and it can also be present in HT eclogites (Bucher and Frey, 2002; Okrusch and Matthes, 2014). Thus, enstatite inclusions are thought to reflect HT conditions during entrapment in garnet.

(iv) Omphacite and coesite inclusions belong to the group of **inclusions which yield specific source rock information**. The mineral assemblage garnet plus omphacite is the diagnostic mineral assemblage of eclogite (e.g., Bucher and Frey, 2002), and therefore omphacite inclusions in garnet directly indicate an eclogitic source. Moreover, the presence of coesite inclusions specifically indicates UHP metamorphic conditions because it is not possible to form coesite inclusions in garnet at conditions lower than the coesite stability field (e.g., Schönig et al., 2018, and references therein).

6.2 Restriction of possible metamorphic source rocks

By combining the information given by the obtained inclusion types in the detrital garnets with the geochemical garnet compositions, the suite of possible source rocks in both catchments can be strongly reduced.

First of all, kyanite inclusions are present in significant amounts of the garnets with ~7% at Flatraket and ~17% at Runde. Due to their abundance, the occurrence in garnets of all obtained geochemical compositions (Figs. 8c, 9c), and the absence of any other aluminosilicate inclusions, all garnet source rocks in the catchments are assumed to be equilibrated in the kyanite stability field. Thus, all metamorphic source rock facies types of the andalusite and sillimanite stability field (contact metamorphism, lowermost greenschist, lower amphibolite, and lower to intermediate granulite facies) can be excluded (field A in Fig. 10b). Note that even in these proximal samples, kyanite made up <2% of the heavy mineral assemblage (Krippner et al., 2016), indicating that this important metamorphic facies index mineral preferably occurs in the form of inclusions in garnet rather than as single mineral in the typical grain-size range of 63–125 μm (or coarser) analyzed in heavy mineral studies. This trend will probably intensify with increasing transport distance because kyanite is mechanically less stable than garnet (e.g., Morton and Hallsworth, 1999).

In the blueschist facies, garnet first appears in the HP part (Bucher and Frey, 2002). If garnet from the sampled catchments would have developed under HP blueschist facies conditions, some typical blueschist facies mineral inclusions like glaucophane or lawsonite would be expected. The absence of these inclusion types, and the high abundance of phlogopite–biotite inclusions (>20% of garnet grains), which are atypical for blueschist facies rocks (Bucher and Frey, 2002), makes blueschist facies rocks unlikely as a garnet source (field B in Fig. 10b). Additionally, the absence of lawsonite inclusions makes a very-low-temperature eclogitic source unlikely (field C in Fig. 10b) because lawsonite inclusions are well known in garnets from lawsonite-eclogites (e.g., Tsujimori et al., 2006, and references therein).

As in the blueschist facies, greenschist facies garnet first appears in the HP part (Bucher and Frey, 2002). Therefore, metamorphic rocks of subgreenschist and lower greenschist facies can be excluded as a garnet source (field D in Fig. 10b). Furthermore, also the HP part of the greenschist facies and the lower amphibolite facies can be excluded (field E in Fig. 10b) due to the very high abundance of rutile inclusions (present in >40%) in garnets of all obtained compositions (Figs. 8c, 9c). Note that although rutile is ultrastable in sedimentary environments, it makes up only <2% of the heavy mineral assemblage (Krippner et al., 2016) but is, besides quartz, the dominant inclusion type in the detrital garnets.

In summary, by considering the conditions where garnet first appears, and the presence/absence of a few inclusion types, the possible source rocks of garnets in both catchments can be reduced to rocks of upper amphibolite, HP granulite, and eclogite facies (excluding very-low-temperature eclogites). This well reflects the experienced conditions of the whole region and the range of outcropping metamorphic rocks in the sampled catchments. Beyond these general constraints, the occurrence of certain mineral inclusions in combination with their preferable host garnet composition reveals some specific catchment characteristics.

6.3 Specific catchment characteristics of Flatraket (AK-N13-1)

The geochemical classification of the garnets from Flatraket implies that by far the most garnets are derived from granulite to eclogite facies source rocks (Fig. 8a). However, a clear separation into different sources by only considering the geochemical composition is not possible.

The fact that eclogite facies rocks are involved as source rocks for parts of the garnets is clearly indicated by the presence of omphacite inclusions in ~8% of the garnets, and an additional indication is given by the presence of diopside inclusions in ~2% of the garnets, which probably have an omphacite (jadeite) component. Most of these garnets are correctly assigned to type A garnets by the multivariate discrimination (Fig. 8d), confirming that the discrimination of eclogite facies garnets works well as reported by Tolosana-Delgado et al. (2017). However, occasionally some of them have the highest probability for type C. This is also highlighted by garnet compositions from the local eclogites determined by Krippner et al. (2016), which mainly have the highest probability of belonging to type A, but garnets from one of the analyzed eclogites also show highest probabilities of belonging to type C (Fig. 8a). Thus, the occurrence of omphacite and diopside inclusions in type C garnets reveals that parts of the type C classified garnets are also derived from eclogite facies rocks. This part can be roughly estimated to be restricted to garnets with a high probability of belonging to type A (>30%), and a small probability of belonging to type B (<12%).

Besides the mineral inclusions which are present in almost all detrital garnets (i.e., quartz, rutile, kyanite, apatite, zircon), the preferable occurrence of epidote and amphibole inclusions in this eclogite facies garnets (Fig. 8e) indicates that these minerals are characteristic for the eclogite facies source rocks. The presence of these hydrous mineral inclusions also makes a granulite facies source improbable. Overall, the deduced mineral assemblage of garnet + omphacite/diopside + epidote + amphibole + rutile + quartz ± kyanite for the eclogite facies garnet type match well with mineral assemblages from eclogites reported from the region of Flatraket (Table 1). An additional sign for a mafic source is the low abundance of alkali feldspar inclusions in these garnets (Fig. 8g).

In addition to the eclogite facies garnets, another large group of garnets are assigned to type C with probabilities ≥12% of belonging to type B. Besides the mineral inclusions which are present in almost all detrital garnets, inclusions of mica group minerals (muscovite–paragonite and phlogopite–biotite) and alkali feldspar are frequent in these garnets, which make a felsic source more probable (Figs. 8f, 8g). Additionally, also quartz and apatite are slightly more frequent (Figs. 8b, 8h), supporting the presumption of a felsic source. This is also highlighted by garnet compositions from the local gneisses determined by Krippner et al. (2016). Garnet composition from the felsic gneiss with a medium garnet content (AK-N13-2d, plotting as type C in Fig. 8a) is very similar to the composition of detrital garnets which are suggested to be of felsic origin. In contrast, no garnets with a comparable composition to the other felsic gneiss (AK-N13-2c, plotting as type B in Fig. 8a) are present in the detritus. This is not surprising, as this gneiss exhibits only a very low garnet content. Overall, it seems reliable that the group of garnets assigned to type C with probabilities ≥12% of belonging to type B are mainly derived from the felsic gneisses. Geochemical characterization favors a granulite facies source, but a precise assignment to a metamorphic facies type by inclusions cannot be specified, because no unique inclusion types for amphibolite-, granulite- and/or eclogite facies exist or were detected.

In summary, the main proportion of detrital garnets is estimated to be derived from eclogites (~55%), whereas the residual garnets (~45%) derived from the felsic gneisses, are probably mainly of granulite facies. Amphibolite facies garnet source rocks play a subordinate role due to their low garnet content.

Considering the different grain-size fractions, the eclogitic garnets are more frequent in the 125–250 µm (~63%) and 250–

500 µm grain-size fraction (~58%), and less frequent in the 63–125 µm fraction (~45%). By contrast, felsic garnets are less frequent in the 125–250 µm (~38%) and 250–500 µm grain-size fraction (~42%), and more abundant in the 63–125 µm fraction (~55%). Although these numbers are only a rough approximation, it is obvious that detrital eclogitic garnets are much more abundant than eclogitic rocks in the catchment area (Fig. 1), and that these are more frequent in the coarser grain-size fractions. Similar observations were made in other regions comprising eclogites in their catchment (e.g., Krippner et al., 2015). Typical factors which quantitatively modify the composition of heavy minerals from source to the sampling location can be widely excluded in the sampled catchment. The high topography and the climatic conditions of the area cause a mainly mechanical weathering of the source rocks. Chemical weathering during transport should be of minor importance due to the high energy of the drainage system and the short transport distance (<4 km). The short transport distance also minimizes the elimination of heavy minerals due to hydraulic effects. Probably the mineralogical composition of the source rocks is the main reason why detrital eclogitic garnets are so prominent. Eclogites mainly consist of omphacite and garnet, and thus supply a much higher amount of heavy minerals to the sedimentary load than felsic rocks compared to their volumetric dimension. Additionally, the heavy mineral assemblage derived

from eclogites (omphacite + garnet) is usually enriched in garnet compared to the assemblage of felsic rocks. The predominant occurrence in the coarser grain-size fractions is probably an effect of inherited grain size due to the short transport distance and the usually large garnet grain size in eclogites.

6.4 Specific catchment characteristics of Runde (AK-N37)

The geochemical classification of the garnets from Runde implies at least two different sources (Fig. 9a). One group shows the highest probabilities for belonging to type A source rocks, agreeing with the geochemical garnet composition from an eclogite located on the island. The other group of garnets gives probabilities of ≤25% for type A and high probabilities for type C (≥35%) with variable type B component. Additionally, several garnets are in the transition zone between these two groups, showing high probabilities for type C and type A.

The fact that eclogite facies source rocks are involved as a source for the garnets of the beach-sediment sample AK-N37 is given by the scarce presence of omphacite inclusions in ~2% of the grains. Presumably, also the garnets containing diopside inclusions (~11%) were derived from eclogite facies rocks, because the diopsides probably have an omphacite (jadeite) component, and eclogites with sodic diopside (13% jadeite) are known from the island of Runde. Garnets containing omphacite are geochemically well assigned to type A, but garnets with diopside inclusions are located in the transition zone between type A and type C (Fig. 9d). The garnets having higher probabilities for type C often contain, besides diopside, also amphibole group mineral inclusions (Fig. 9e), which makes an affiliation to granulite facies source rocks (type C) less probable. This also means that at least some of the enstatite-bearing garnets (Fig. 9d), which additionally often contain diopside and/or amphibole group inclusions, probably do not originate from granulite facies rocks. Instead, the coexistence of garnet + omphacite/diopside + amphibole + enstatite, and the absence of epidote group minerals, favors a high-temperature eclogitic source for the garnets with highest probabilities of belonging to type C but which also have high probabilities for type A. However, caution should be taken when considering more than one inclusion, but in general, the higher temperatures supposed for the source rocks of the garnets from Runde compared to Flatraket are in agreement with the estimated higher peak metamorphic temperatures of the region (Fig. 1). Additionally, the low frequency of alkali feldspar and quartz inclusions in these garnets supports a mafic source. Thus, also the garnets in the transition zone between the two groups of garnets are assigned to the eclogitic source.

The other group of garnets with probabilities of ≤25% for type A and high probabilities for type C (≥35%) are characterized by an increased occurrence of alkali feldspar, quartz, rutile, and phlogopite–biotite, favoring a felsic source. There is no coincidence with geochemical garnet compositions from the gneiss reported by Krippner et al. (2016) (Fig. 9a), which was to be expected because the sampled gneiss unit (AK-N39-1) is only located at the outermost part of the catchment (Fig. 1). Probably the garnets mainly derived from the micaceous quartzo-feldspathic gneiss, which is the main rock type of the catchment.

Moreover, from the coesite inclusions in two garnets assigned to the felsic source (Fig. 9b), and the coesite inclusions reported by Schönig et al. (2018), which can be assigned to the felsic and the eclogitic source (including garnets of the transition zone), it is indisputable that at least parts of some felsic source rocks experienced UHP metamorphic conditions.

In summary, the main portion of detrital garnets is estimated to be derived from eclogites (~57%), which probably equilibrated under higher temperatures than that located in the catchment of Flatraket. Another large portion of garnets (~36%) is assigned to felsic source rocks, which are mainly assigned to granulite facies and to a lesser extent to upper amphibolite facies. Source rocks of the residual ~7% cannot be specified, and are thus assigned to source rocks of upper amphibolite facies or higher.

Considering the different grain-size fractions, the supposed eclogitic garnets are more frequent in the 125–250 µm grain-size fraction (~65%), and less frequent in the 63–125 µm (~57%) and 250–500 µm fraction (~54%). Contrary, felsic garnets are less frequent in the 125–250 µm grain-size fraction (~27%), and more abundant in the 63–125 µm (~36%) and 250–500 µm fraction (~42%). Overall, at Runde eclogitic garnets are much more frequent than eclogitic rocks in the catchments due to the mineralogical composition of eclogites, but the grain-size effect is less pronounced than at Flatraket.

7. Conclusions and Outlook

The results of this detailed study using mineral inclusions in garnet as provenance indicator show that by far the most garnets from HP/UHP metamorphic source rocks contain mineral inclusions ≥2 µm. To identify these tiny mineral inclusions in the entire volume of a garnet grain, Raman spectroscopy is a very powerful tool. Some minerals, however, cannot be easily specified precisely, and therefore have to be compiled into mineral groups.

Potential metamorphic source rocks for the analyzed detrital garnets can be significantly reduced by considering the conditions where garnet first appears (upper blueschist and upper greenschist facies), and the presence/absence of a few inclusion types. Especially the presence of kyanite and rutile inclusions in garnets of all chemical compositions, the absence of other aluminosilicate inclusions, and the absence of blueschist facies mineral inclusions (glaucophane, lawsonite) lead to the restriction to rocks of upper amphibolite, HP granulite, and eclogite facies as a possible source.

Moreover, the presence of eclogite facies rocks in the catchments could be verified by the presence of omphacite inclusions, and also by the presence of diopside inclusions which probably have an omphacite (jadeite) component. In the catchment of Runde, the presence of coesite inclusions in the detrital garnets further verifies an involvement of UHP metamorphic rocks, including mafic and felsic compositions.

The combination of single inclusion data, coexisting mineral inclusions, and geochemical data allows a portioning of the detrital garnets into source rock groups, which goes beyond the classical geochemical classification. As a result, garnets with high probabilities for more than one host-rock group can be more confidently assigned to one of the groups, and additionally, some information can be gained about protolith composition (mafic vs. felsic) and coexisting mineral phases.

Overall, the mineral inclusions, especially in combination with geochemical host garnet composition, well reflect the geological characteristics of the sampled catchments, implying that they are useful indicators for HP/UHP provenance. Several of the most meaningful inclusion types in this study like kyanite, omphacite, diopside, enstatite, coesite, amphibole group, and epidote group minerals are either chemically and/or mechanically less stable than garnet. Thus, garnet can shield these inclusions from processes of the sedimentary cycle and preserve the mineralogical information as long as garnet is stable. This becomes more and more important when looking for HP/UHP provenance in less proximal, buried, and/or recycled sediments and sedimentary rocks. Furthermore, some provenance indicator minerals like kyanite and rutile seem to occur much more frequently as inclusions in garnet than as single grains in the heavy mineral assemblage, making inclusion analysis to a preferred tool when looking for these minerals.

The use of mineral inclusions in detrital garnet as a provenance tool has wide implications for prospective investigations. In particular, the contribution of material sourced from HP/UHP metamorphic rocks, which has significant geologic and geodynamic implications, can be determined more confidently than by using existing techniques. In contrast to conventional heavy mineral studies, where individual mineral grains are not in contact to each other, mineral assemblages deduced from inclusions can be directly transmitted into metamorphic mineral assemblages (minerals in mutual grain contact). Thereby, the preservation of HP/UHP index minerals from retrograde metamorphic stages and processes of the sedimentary cycle by the garnet host constitutes a major advantage. Compared to geochemical garnet single-grain analysis, where an assignment to a specific source rock is often limited to statistical probabilities, the introduced approach can provide direct mineralogical evidence for HP/UHP sources unbiased from the geochemical garnet composition. Moreover, the possibility of discriminating UHP garnets is not yet given by any other discrimination scheme.

Due to the mentioned advantages and the abundance of garnet in sediments sourced from metamorphic rocks, the introduced approach is thought to become a frequently used and valuable tool in sedimentary provenance analysis. The limiting factor at present is the analytical time needed. However, in combination with geochemical discrimination schemes, analyzing the inclusions in a much smaller quantity of pre-selected grains, with compositions likely reflecting a specific source, would reduce the analytical time significantly. Further acceleration of analysis is expected by the rapid technical development of Raman spectrometry, allowing shorter acquisition times and automated measurement routines.

Acknowledgements

This study is partially based on precursor work in the Western Gneiss Region financially supported by CASP (formerly known as Cambridge Arctic Shelf Programme) and the Deutsche Forschungsgemeinschaft (DFG grant EY 23/20-1). This research did not receive any further specific grant from funding agencies in the public, commercial, or not-for-profit sectors. We thank A. Krippner for assistance in the field and the contribution to early steps of the sample preparation sequence. We thank J. E. Dunkelné Nagy, I. Dunkl, K. Löwen, and A. Grebe for their support in sample preparation. A. Kronz is thanked for providing access to the electron microprobe and his help during microprobe analysis. Helpful comments from Sergio Andò, an anonymous reviewer, and the editor Jasper Knight on an earlier draft of the manuscript are gratefully acknowledged.

Appendices

Supplementary Tables 1–6 can be found online as Supplementary Data at http://xxxxx

References

Andersen, T.B., Skjerlie, K.P., Furnes, H., 1990. The Sunnfjord Melange, evidence of Silurian ophiolite accretion in the west Norwegian Caledonides. Journal of the Geological Society 147, 59–68.

Andò, S., Garzanti, E., 2014. Raman spectroscopy in heavy-mineral studies. In: Scott, R.A., Smyth, H.R., Morton, A.C., Richardson, N. (Eds.), Sediment Provenance Studies in Hydrocarbon Exploration and Production. Geological Society of London, Special Publications 386, pp. 395–412.

Apopei, A.I., Buzgar, N., 2010. The Raman study of amphiboles. Analele Stiintifice de Universitatii AI Cuza din Iasi. Section 2, Geologie 56, 57–83.

Bersani, D., Aliatis, I., Tribaudino, M., Mantovani, L., Benisek, A., Carpenter, M.A., Gatta, G.D., Lottici, P.P., 2018. Plagioclase composition by Raman spectroscopy. Journal of Raman Spectroscopy 49, 684–698.

Beyer, E.E., Brueckner, H.K., Griffin, W.L., O'Reilly, S.Y., 2012. Laurentian Provenance of Archean Mantle Fragments in the Proterozoic Baltic Crust of the Norwegian Caledonides. Journal of Petrology 53, 1357–1383.

Bingen, B., Davis, W.J., Austrheim, H., 2001. Zircon U–Pb geochronology in the Bergen arc eclogites and their Proterozoic protoliths, and implications for the pre-Scandian evolution of the Caledonides in western Norway. Geological Society of America Bulletin 113, 640–649.

Bohlen, S.R., Montana, A., Kerrick, D.M., 1991. Precise determinations of the equilibria kyanite–sillimanite and kyanite–andalusite and a revised triple point for Al_2SiO_5 polymorphs. American Mineralogist 76, 677–680.

Bucher, K., Frey, M., 2002. Petrogenesis of Metamorphic Rocks. Springer-Verlag, Berlin-Heidelberg.

Buzatu, A., Buzgar, N., 2010. The Raman study of single-chain silicates. Analele Stiintifice de Universitatii AI Cuza din Iasi. Section 2, Geologie 56, 107–125.

Carswell, D.A., Cuthbert, S.J., 2003. Review of the mineralogical and microstructural evolution of ultra-high pressure eclogites in the Western Gneiss region. In: Carswell, D.A., Cuthbert, S.J., Krabbendam, M., Medaris, L.G., Brueckner, H.K., Eide, E.A. (Eds.), Guidebook to the field excursions in the Nordfjord-Stadtlandet-Almklovdalen area. Geological Survey of Norway, Trondheim, pp. 3–47.

Corfu, F., Austrheim, H., Ganzhorn, A.C., 2014. Localized granulite and eclogite facies metamorphism at Flatraket and Kråkeneset, Western Gneiss Region: U–Pb data and tectonic implications. In: Corfu, F., Gasser, D., Chew, D.M. (Eds.), New Perspectives on the Caledonides of Scandinavia and Related Areas. Geological Society of London, Special Publications 390, pp. 425–442.

Dahl, E., 1954. Weathered gneisses at the Island of Runde, Sunnmøre, Western Norway, and their geological interpretation. Nytt Magasin for Botanik 3, 5–23.

Faryad, S.W., Nahodilová, R., Dolejš, D., 2010. Incipient eclogite facies metamorphism in the Moldanubian granulites revealed by mineral inclusions in garnet. Lithos 114, 54–69.

Force, E.R., 1980. The provenance of rutile. Journal of Sedimentary Research 50, 485–488.

Freeman, J.J., Wang, A., Kuebler, K.E., Jolliff, B.L., Haskin, L.A., 2008. Characterization of natural feldspars by Raman spectroscopy for future planetary exploration. The Canadian Mineralogist 46, 1477–1500.

Goksøyr, H., 1938. Das Pfanzenleben auf Rundøy, Sunnmøre in Norwegen. I Kommisjon hos Jacob Dybwad, Oslo.

Griffin, W.L., Austrheim, H., Brastad, K., Bryhni, I., Krill, A.G., Krogh, E.J., Mørk, M.B., Qvale, H., Tørudbakken, B., 1985. High-pressure metamorphism in the Scandinavian Caledonides. In: Gee, D.G., Sturt, B.A. (Eds.), The Caledonide orogen – Scandinavia and related areas. John Wiley & Sons, Chichester, pp. 783–801.

Guiraud, M., Powell, R., 2006. P–V–T relationships and mineral equilibria in inclusions in minerals. Earth and Planetary Science Letters 244, 683–694.

Hacker, B.R., Andersen, T.B., Johnston, S., Kylander-Clark, A.R.C., Peterman, E.M., Walsh, E.O., Young, D., 2010. High-temperature deformation during continental-margin subduction and exhumation: The ultrahigh-pressure Western Gneiss Region of Norway. Tectonophysics 480, 149–171.

Hughes, A.L., Gyllencreutz, R., Lohne, Ø.S., Mangerud, J., Svendsen, J.I., 2016. The last Eurasian ice sheets – a chronological database and time-slice reconstruction, DATED-1. Boreas 45, 1–45.

Krabbendam, M., Wain, A., 1997. Late-Caledonian structures, differential retrogression and structural position of (ultra) high-pressure rocks in a Nordfjord-Stadlandet area, Western Gneiss Region. Norges geologiske undersøkelse 432, 127–139.

Krabbendam, M., Wain, A., Andersen, T.B., 2000. Pre-Caledonian granulite and gabbro enclaves in the Western Gneiss Region, Norway: indications of incomplete transition at high pressure. Geological Magazine 137, 235–255.

Krippner, A., Meinhold, G., Morton, A.C., von Eynatten, H., 2014. Evaluation of garnet discrimination diagrams using geochemical data of garnets derived from various host rocks. Sedimentary Geology 306, 36–52.

Krippner, A., Meinhold, G., Morton, A.C., Russell, E., von Eynatten, H., 2015. Grain-size dependence of garnet composition revealed by provenance signatures of modern stream sediments from the western Hohe Tauern (Austria). Sedimentary Geology 321, 25–38.

Krippner, A., Meinhold, G., Morton, A.C., von Eynatten, H., 2016. Heavy-mineral and garnet compositions of stream sediments and HP–UHP basement rocks from the Western Gneiss Region, SW Norway. Norwegian Journal of Geology 96, 7–17.

Krogh, E.J., 1977. Evidence of Precambrian continent-continent collision in Western Norway. Nature 267, 17–19.

Krogh, E.J., 1982. Metamorphic evolution of Norwegian country-rock eclogites, as deduced from mineral inclusions and compositional zoning in garnets. Lithos 15, 305–321.

Kylander-Clark, A.R.C., Hacker, B.R., Mattinson, J.M., 2008. Slow exhumation of UHP terranes: titanite and rutile ages of the Western Gneiss Region, Norway. Earth and Planetary Science Letters 272, 531–540.

Laetsch, T., Downs, R., 2006. Software for identification and refinement of cell parameters from powder diffraction data of minerals using the RRUFF project and American mineralogist crystal structure databases. 19th General Meeting of the International Mineralogical Association. International Mineralogical Association, Kobe, Japan, p. 152.

Lafuente, B., Downs, R.T., Yang, H., Stone, N., 2015. The power of databases: The RRUFF project. In: Armbruster, T., Danisi, R.M. (Eds.), Highlights in Mineralogical Crystallography. De Gruyter, Berlin, pp. 1–30.

Leissner, L., Schlüter, J., Horn, I., Mihailova, B., 2015. Exploring the potential of Raman spectroscopy for crystallochemical analyses of complex hydrous silicates: I. Amphiboles. American Mineralogist 100, 2682–2694.

Mangerud, J., 2004. Ice sheet limits on Norway and the Norwegian continental shelf. In: Ehlers, J., Gibbard, P.L. (Eds.), Quaternary Glaciations—Extent and Chronology, Part I: Europe. Elsevier, Amsterdam, pp. 271–294.

Mernagh, T.P., 1991. Use of the laser Raman microprobe for discrimination amongst feldspar minerals. Journal of Raman Spectroscopy 22, 453–457.

Mernagh, T.P., Hoatson, D.M., 1997. Raman spectroscopic study of pyroxene structures from the Munni Munni layered intrusion, Western Australia. Journal of Raman Spectroscopy 28, 647–658.

Morton, A.C., Hallsworth, C.R., 1999. Processes controlling the composition of heavy mineral assemblages in sandstones. Sedimentary Geology 124, 3–29.

Nasdala, L., Smith, D.C., Kaindl, R., Ziemann, M.A., 2004. Raman spectroscopy: analytical perspectives in mineralogical research. Spectroscopic Methods in Mineralogy 6, 281–343.

Neuville, D.R., de Ligny, D., Henderson, G.S., 2014. Advances in Raman spectroscopy applied to Earth and Material Sciences. Reviews in Mineralogy and Geochemistry 78, 509–541.

Okrusch, M., Matthes, S., 2014. Mineralogie: Eine Einführung in die spezielle Mineralogie, Petrologie und Lagerstättenkunde. Springer-Verlag, Berlin-Heidelberg.

Peterman, E.M., Hacker, B.R., Baxter, E.F., 2009. Phase transformations of continental crust during subduction and exhumation: Western Gneiss Region, Norway. European Journal of Mineralogy 21, 1097–1118.

Roberts, D.C., Gee, D.G., 1985. An introduction to the structure of the Scandinavian Caledonides. In: Gee, D.G., Sturt, B.A. (Eds.), The Caledonide orogen – Scandinavia and related areas. John Wiley & Sons, Chichester, pp. 55–68.

Røhr, T.S., Corfu, F., Austrheim, H., Andersen, T.B., 2004. Sveconorwegian U–Pb zircon and monazite ages of granulite-facies rocks, Hisaroya, Gulen, Western Gneiss Region, Norway. Norsk Geologisk Tidsskift 84, 251–256.

Root, D.B., Hacker, B.R., Mattinson, J.M., Wooden, J.L., 2004. Zircon geochronology and ca. 400 Ma exhumation of Norwegian ultrahigh-pressure rocks: an ion microprobe and chemical abrasion study. Earth and Planetary Science Letters 228, 325–341.

Root, D.B., Hacker, B.R., Gans, P.B., Ducea, M.N., Eide, E.A., Mosenfelder, J.L., 2005. Discrete ultrahigh-pressure domains in the Western Gneiss Region, Norway: implications for formation and exhumation. Journal of Metamorphic Geology 23, 45–61.

Rye, N., Nesje, A., Lien, R., Anda, R., 1987. The Late Weichselian ice sheet in the Nordford–Sunnmøre area and deglaciation chronology for Nordford, western Norway. Norsk Geologisk Tidsskift 41, 23–43.

Scambelluri, M., Pettke, T., van Roermund, H., 2008. Majoritic garnets monitor deep subduction fluid flow and mantle dynamics. Geology 36, 59–62.

Schönig, J., Meinhold, G., von Eynatten, H., Lünsdorf, N.K., 2018. Tracing ultrahigh pressure metamorphism at the catchment scale. Scientific Reports 8, 2931, doi:10.1038/s41598-018-21262-8.

Smith, D.C., 1984. Coesite in clinopyroxene in the Caledonides and its implications for geodynamics. Nature 310, 641–644.

Smith, D.C., 1985. Coesite in the Straumen eclogite pod, Norway. Terra Cognita 5, 226–227.

Smith, D.C., 1995. Microcoesites and Microdiamonds in Norway: An Overview. In: Coleman, R.G., Wang, X. (Eds.), Ultrahigh Pressure Metamorphism. Cambridge University

Press, Cambridge, pp. 299–355.Smith, D.C., Godard, G., 2013. A Raman spectroscopic study of diamond and disordered sp3-carbon in the coesite-bearing Straumen Eclogite Pod, Norway. Journal of Metamorphic Geology 31, 19–33.

Spencer, K.J., Hacker, B.R., Kylander-Clark, A.R.C., Andersen, T.B., Cottle, J.M., Stearns, M.A., Poletti, J.E., Seward, G.G., 2013. Campaign-style titanite U–Pb dating by laser-ablation ICP: implications for crustal flow, phase transformations and titanite closure. Chemical Geology 341, 84–101.

Spengler, D., Brueckner, H.K., van Roermund, H., Drury, M.R., Mason, P.R.D., 2009. Long-lived, cold burial of Baltica to 200 km depth. Earth and Planetary Science Letters 281, 27–35.

Thompson, A.B., Tracy, R.J., Lyttle, P.T., Thompson, J.B., 1977. Prograde reaction histories deduced from compositional zonation and mineral inclusions in garnet from the Gassetts schist, Vermont. American Journal of Science 277, 1152–1167.

Thoresen, M.K., 2013. Kvartærgeologisk kart over Norge. Tema: Jordarter. M 1:1 mill., revidert 3. opplag. Norges geologiske undersøkelse, Trondheim.Tolosana-Delgado, R., von Eynatten, H., Krippner, A., Meinhold, G., 2017. A multivariate discrimination scheme of detrital garnet chemistry for use in sedimentary provenance analysis. Sedimentary Geology, https://doi.org/10.1016/j.sedgeo.2017.11.003.

Torsvik, T.H., Cocks, L.R.M., 2005. Norway in space and time: a centennial cavalcade. Norwegian Journal of Geology 85, 73–86.

Tsujimori, T., Sisson, V.B., Liou, J.G., Harlow, G.E., Sorensen, S.S., 2006. Very-low temperature record of the subduction process: A review of worldwide lawsonite eclogites. Lithos 92, 609–624.

Undås, I., 1942. On the Late-Quaternary history of Møre and Trøndelag (Norway). Det Kongelige Norske Videnskapers-Selskap Skrifter 2, 1–92.

van den Kerkhof, A.M., Hein, U.F., 2001. Fluid inclusion petrography. Lithos 55, 27–47.

van Roermund, H., 2009. Recent progress in Scandian ultrahigh-pressure metamorphism in the northernmost domain of the Western Gneiss Complex, SW Norway: continental subduction down to 180–200 km depth. Journal of the Geological Society 166, 739–751.

Wain, A., 1997. New evidence for coesite in eclogite and gneisses: Defining an ultrahigh-pressure province in the Western Gneiss region of Norway. Geology 25, 927–930.

Wain, A., Waters, D.J., Jephcoat, A., Olijynk, H., 2000. The high-pressure to ultrahigh-pressure eclogite transition in the Western Gneiss Region, Norway. European Journal of Mineralogy 12, 667–687.

Wain, A.L., Waters, D.J., Austrheim, H., 2001. Metastability of granulites and processes of eclogitisation in the UHP region of western Norway. Journal of Metamorphic Geology 19, 609–625.

Walsh, E.O., Hacker, B.R., 2004. The fate of subducted continental margins: Two-stage exhumation of the high-pressure to ultrahigh-pressure Western Gneiss Region, Norway. Journal of Metamorphic Geology 22, 671–687.

Walsh, E.O., Hacker, B.R., Gans, P.B., Wong, M.S., Andersen, T.B., 2013. Crustal exhumation of the Western Gneiss Region UHP terrane, Norway: $^{40}Ar/^{39}Ar$ thermochronology and fault-slip analysis. Tectonophysics 608, 1159–1179.

Wang, A., Jolliff, B.L., Haskin, L.A., Kuebler, K.E., Viskupic, K.M., 2001. Characterization and comparison of structural and compositional features of planetary quadrilateral pyroxenes by Raman spectroscopy. American Mineralogist 86, 790–806.

Wang, A., Freeman, J.J., Jolliff, B.L., 2015. Understanding the Raman spectral features of phyllosilicates. Journal of Raman Spectroscopy 46, 829–845.

Zack, T., von Eynatten, H., Kronz, A., 2004. Rutile geochemistry and its potential use in quantitative provenance studies. Sedimentary Geology 171, 37–58.

Tables

Table 1. Compilation of mineral assemblages from metamorphic rocks occurring in the Flatraket catchment (sample AK-N13-1) and its close vicinity. Mineralogical data according to [1]Krabbendam et al. (2000), [2]Wain (1997), [3]Root et al. (2004), and [4]Smith (1995). Abbreviations: Grt – garnet; Qz – quartz; Coe – coesite; Rt – rutile; Afs – alkali feldspar; Pl – plagioclase; Wmca – white mica; Phl–Bt – phlogopite–biotite; Omp – omphacite; Aug – augite; Opx – orthopyroxene group; Amp – amphibole group; Ky – kyanite; Ep – epidote group; Cb – carbonate minerals.

Figure captions

Fig. 1. Location map and geological map of the sampling areas (modified from Krippner et al., 2016). The left side shows an overview map of the region around Faltraket and Runde (indicated by the red boxes), including an inset marking the map section (black box), location of the UHP domains according to Root et al. (2005), and peak metamorphic temperature isolines according to Kylander-Clark et al. (2008).

Right side shows the geology of the two sampling areas and the location of the sediment, crystalline rock, and pebble samples.

Fig. 2. Example of isolating an inclusion spectrum from the inclusion/host mixed spectrum by means of a zircon inclusion in one of the host garnets. For isolation, the garnet host spectrum captured directly next to the inclusion (blue) gets subtracted from the inclusion/host mixed spectrum (red). This results in an isolated spectrum of the inclusion (green).

Fig. 3. Examples of different inclusion spectra from the samples AK-N13-1 and AK-N37. Oxides (a – SiO_2 polymorphs quartz and coesite; b – rutile), nesosilicates (c – kyanite; d – zircon), the phosphate apatite (e), and feldspars (f – blueish spectra plagioclase and reddish spectra alkali feldspar). Bands of the host garnets are labeled with ‘Grt’.

Fig. 4. Spectra of phyllosilicate inclusions giving the highest probabilities for phlogopite (blueish spectra) and muscovite (reddish spectra) by comparison with the RRUFF database.

Fig. 5. Spectra of clinopyroxene (a), orthopyroxene (b), and amphibole inclusions (c). Clinopyroxene spectra (a) of 9 inclusions in the analyzed garnets are shown, compared with spectra from the RUFF database (diopside: ID 040009, ID 060171; omphacite: ID 061129.2) and an omphacite in the UHP eclogite at Flatraket harbor (AK-N12).

Fig. 6. Proportion of host garnets from the stream-sediment sample of Flatraket (AK-N13-1) containing specific inclusion types (see 5.1.1) as a function of grain-size fraction (also listed in Supplementary Table 2, and more detailed in Supplementary Table 1).

Fig. 7. Proportion of host garnets from the beach-sediment sample of Runde (AK-37) containing specific inclusion types (see 5.1.1) as a function of grain-size fraction (also listed in Supplementary Table 4, and more detailed in Supplementary Table 3).

Fig. 8. Probabilities for the detrital host garnets from Flatraket (AK-N13-1) of belonging to the major metamorphic host-rock groups (A – eclogite facies rocks; B – amphibolite facies rocks; C – granulite facies rocks), based on geochemical composition and the calculation according to Tolosana-Delgado et al. (2017) (Supplementary Table 6). (a**)** – probabilities for all analyzed garnets divided in grain-size fractions (same symbols are used in (**b–i)**). Additionally, the probabilities for some local crystalline rocks are given, based on Krippner et al. (2016). (b–i) – probabilities for garnets containing specific mineral inclusion types. Pie charts are showing the proportion of grains with the highest probability of belonging to one of the major metamorphic host-rock groups (A, B, or C) for the entire grain-size fraction (63–500 µm).

Fig. 9. Probabilities for the detrital host garnets from Runde (AK-N37) of belonging to the major metamorphic host-rock groups (A – eclogite facies rocks; B – amphibolite facies rocks; C – granulite facies rocks), based on geochemical composition and the calculation according to Tolosana-Delgado et al. (2017) (Supplementary Table 6). (a) – probabilities for all analyzed garnets divided in grain-size fractions (same symbols are used in (b–i)). Additionally, the probabilities for some local crystalline rocks are given, based on Krippner et al. (2016). (b–i) – probabilities for garnets containing specific mineral inclusion types. Pie charts are showing the proportion of grains with the highest probability of belonging to one of the major metamorphic host-rock groups (A, B, or C) for the entire grain-size fraction (63–500 µm).

Fig. 10. Metamorphic facies diagram. (a) *P–T* regions of metamorphic facies types adopted from Bucher and Frey (2002), which were extended to ultrahigh-pressure (UHP) conditions. Stability fields for quartz/coesite adopted from Guiraud and Powell (2006), and stability fields for aluminosilicates kyanite/sillimanite/andalusite adopted from Bohlen et al. (1991) and linearly extended (dashed line). (b) Metamorphic facies types which can be excluded as a source for the analyzed detrital garnets (grey fields: A–D). A: Facies types of the andalusite and sillimanite stability field (contact metamorphism, lowermost greenschist, lower amphibolite, and

lower to intermediate granulite facies); B: Blueschist facies rocks; C: Very-low-temperature eclogites (lawsonite-eclogites); D: Subgreenschist and lower greenschist facies rocks; E: Upper greenschist and lower amphibolite facies rocks.

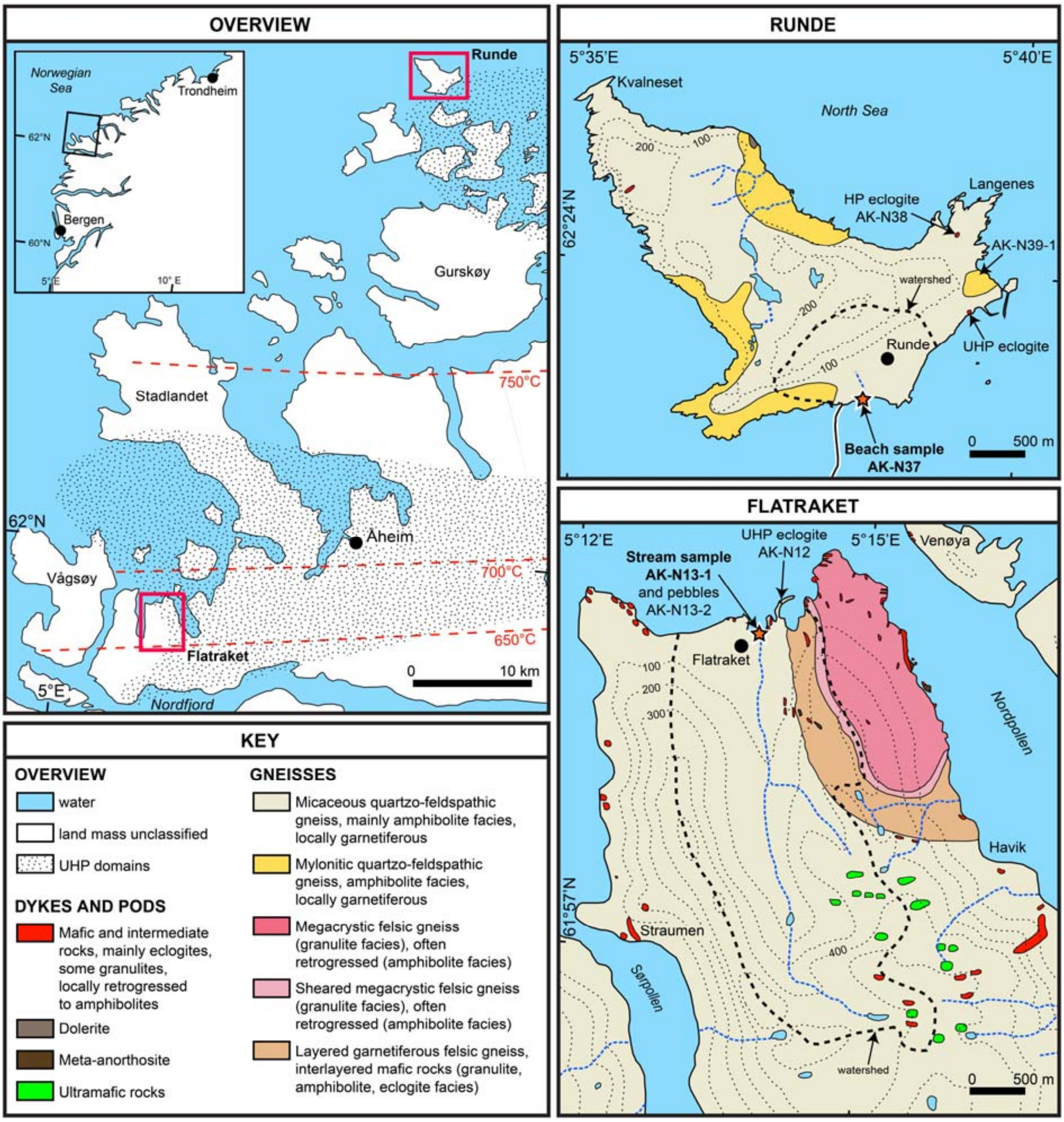

OVERVIEW
Norwegian Sea
Trondheim
Bergen
62°N
60°N
5°E
10° E
Runde
Gurskøy
Stadlandet
750°C
700°C
650°C
62°N
Åheim
Vågsøy
Flatraket
5°E
Nordfjord
0 10 km
RUNDE
5°35'E
5°40'E
62°24'N
Kvalneset
North Sea
Langenes
HP eclogite AK-N38
AK-N39-1
watershed
UHP eclogite
Runde
Beach sample AK-N37
0 500 m
FLATRAKET
5°12'E
5°15'E
Venøya
Stream sample AK-N13-1 and pebbles AK-N13-2
UHP eclogite AK-N12
Flatraket
Nordpollen
Havik
61°57'N
Straumen
Sørpollen
watershed
0 500 m
KEY
OVERVIEW
water
land mass unclassified
UHP domains
DYKES AND PODS
Mafic and intermediate rocks, mainly eclogites, some granulites, locally retrogressed to amphibolites
Dolerite
Meta-anorthosite
Ultramafic rocks
GNEISSES
Micaceous quartzo-feldspathic gneiss, mainly amphibolite facies, locally garnetiferous
Mylonitic quartzo-feldspathic gneiss, amphibolite facies, locally garnetiferous
Megacrystic felsic gneiss (granulite facies), often retrogressed (amphibolite facies)
Sheared megacrystic felsic gneiss (granulite facies), often retrogressed (amphibolite facies)
Layered garnetiferous felsic gneiss, interlayered mafic rocks (granulite, amphibolite, eclogite facies)

Fig. 1

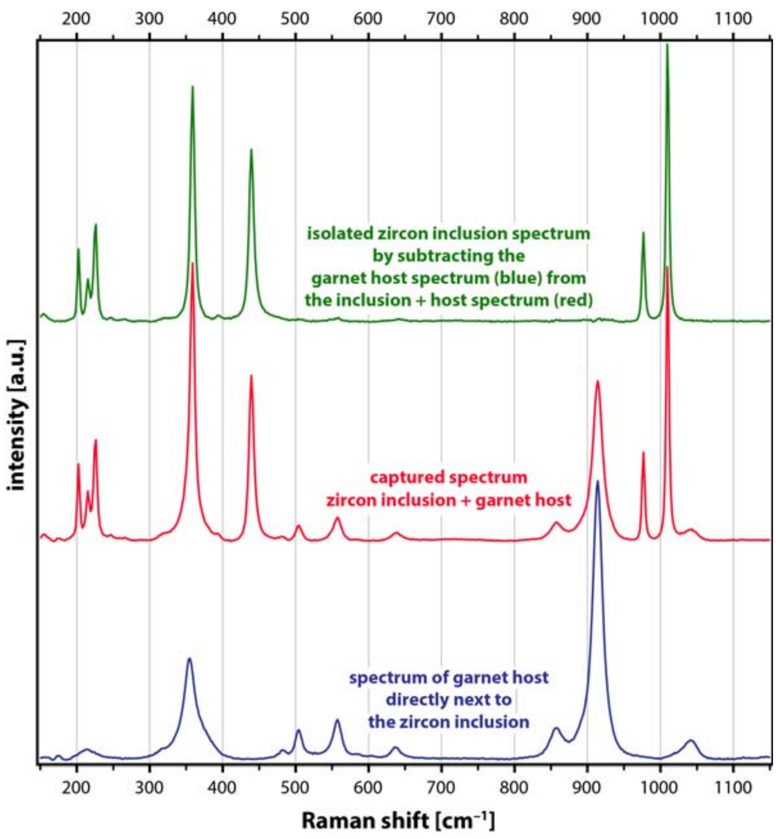
isolated zircon inclusion spectrum
by subtracting the
garnet host spectrum (blue) from
the inclusion + host spectrum (red)
captured spectrum
zircon inclusion + garnet host
spectrum of garnet host
directly next to
the zircon inclusion
intensity [a.u.]
Raman shift [cm⁻¹]
200
300
400
500
600
700
800
900
1000
1100

Fig. 2

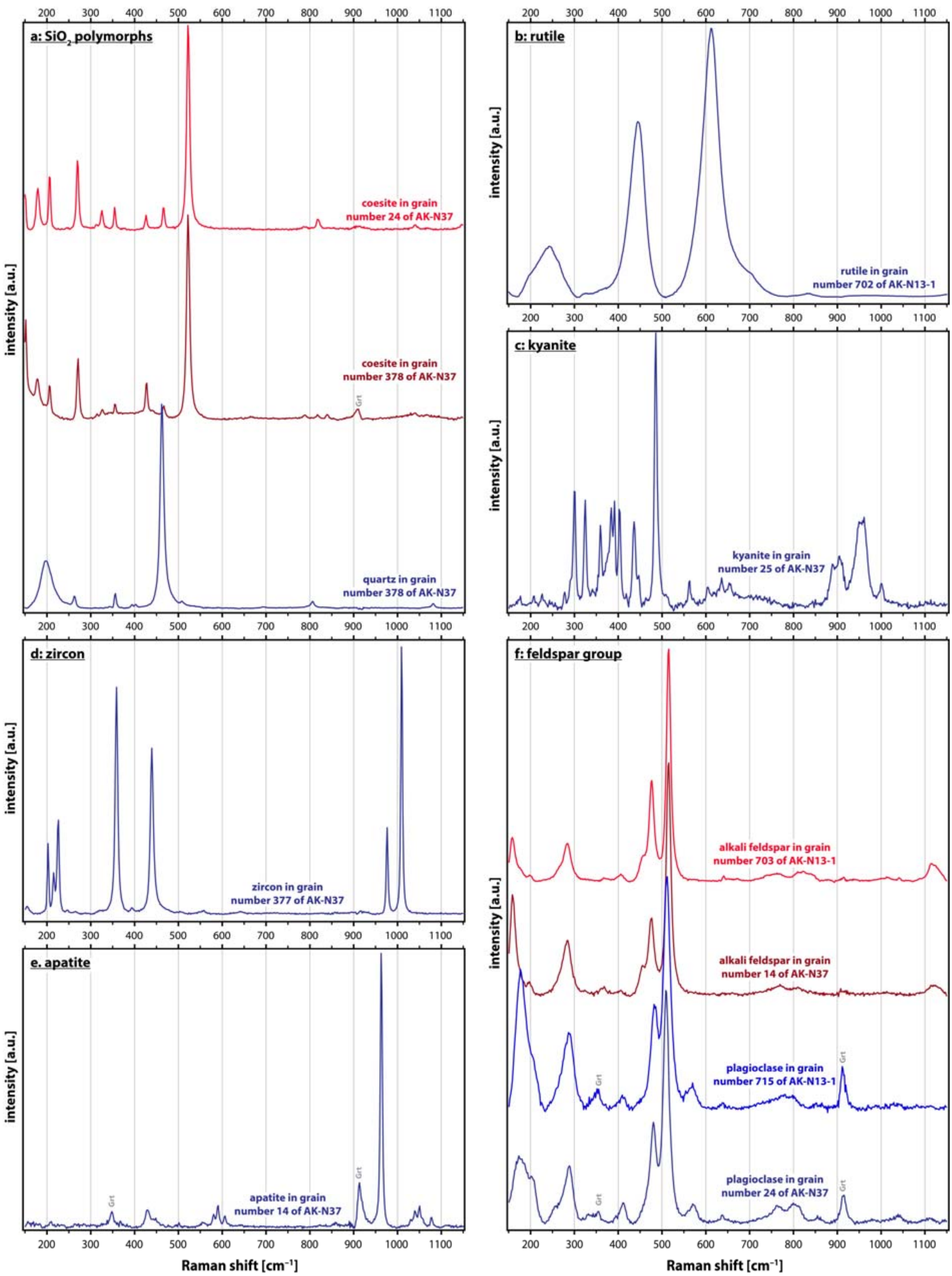

a: SiO$_2$ polymorphs
coesite in grain number 24 of AK-N37
coesite in grain number 378 of AK-N37
quartz in grain number 378 of AK-N37
Grt
b: rutile
rutile in grain number 702 of AK-N13-1
c: kyanite
kyanite in grain number 25 of AK-N37
d: zircon
zircon in grain number 377 of AK-N37
e. apatite
apatite in grain number 14 of AK-N37
f: feldspar group
alkali feldspar in grain number 703 of AK-N13-1
alkali feldspar in grain number 14 of AK-N37
plagioclase in grain number 715 of AK-N13-1
plagioclase in grain number 24 of AK-N37
intensity [a.u.]
Raman shift [cm^{-1}]

Fig. 3

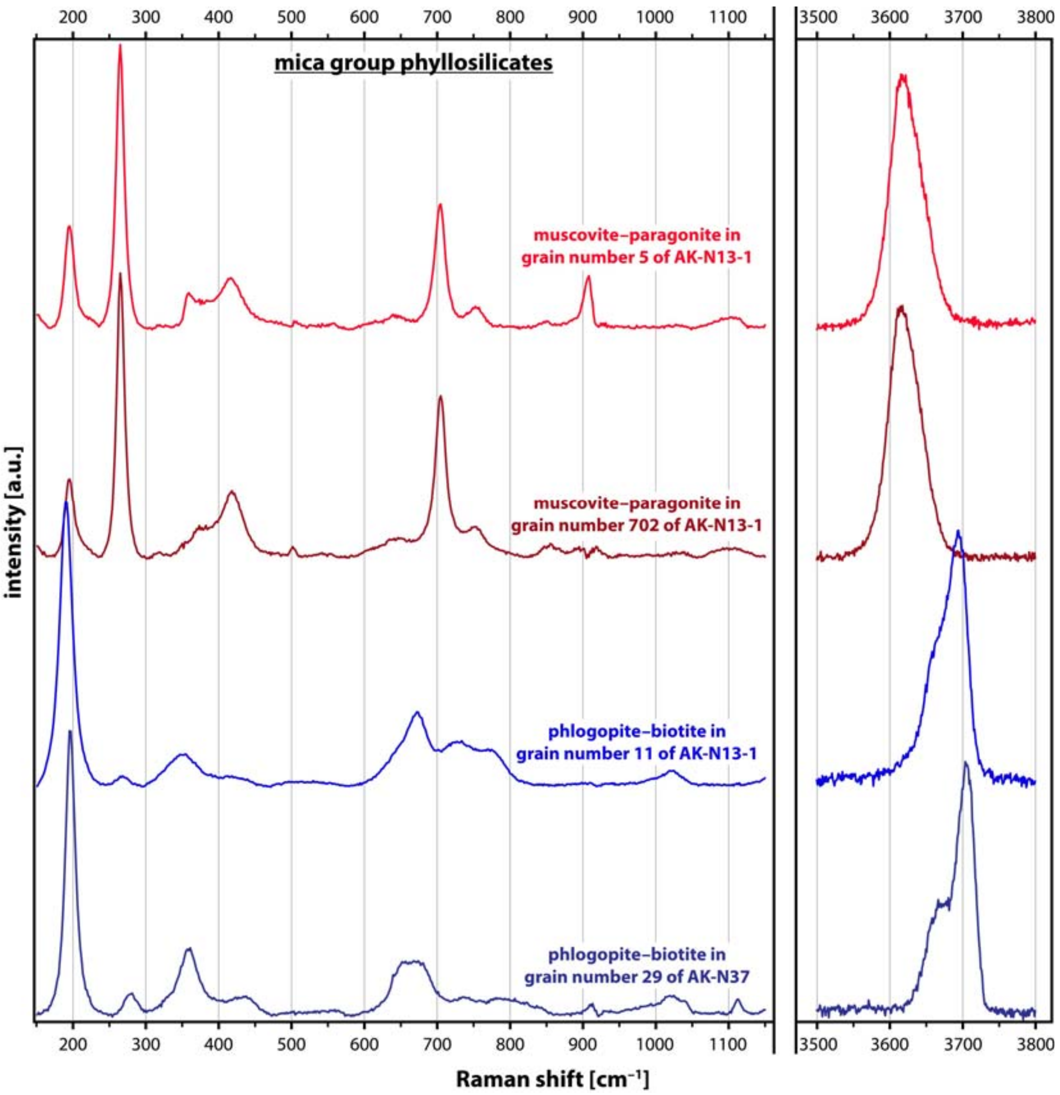

mica group phyllosilicates
muscovite–paragonite in grain number 5 of AK-N13-1
muscovite–paragonite in grain number 702 of AK-N13-1
phlogopite–biotite in grain number 11 of AK-N13-1
phlogopite–biotite in grain number 29 of AK-N37
intensity [a.u.]
Raman shift [cm⁻¹]
200 300 400 500 600 700 800 900 1000 1100
3500 3600 3700 3800

Fig. 4

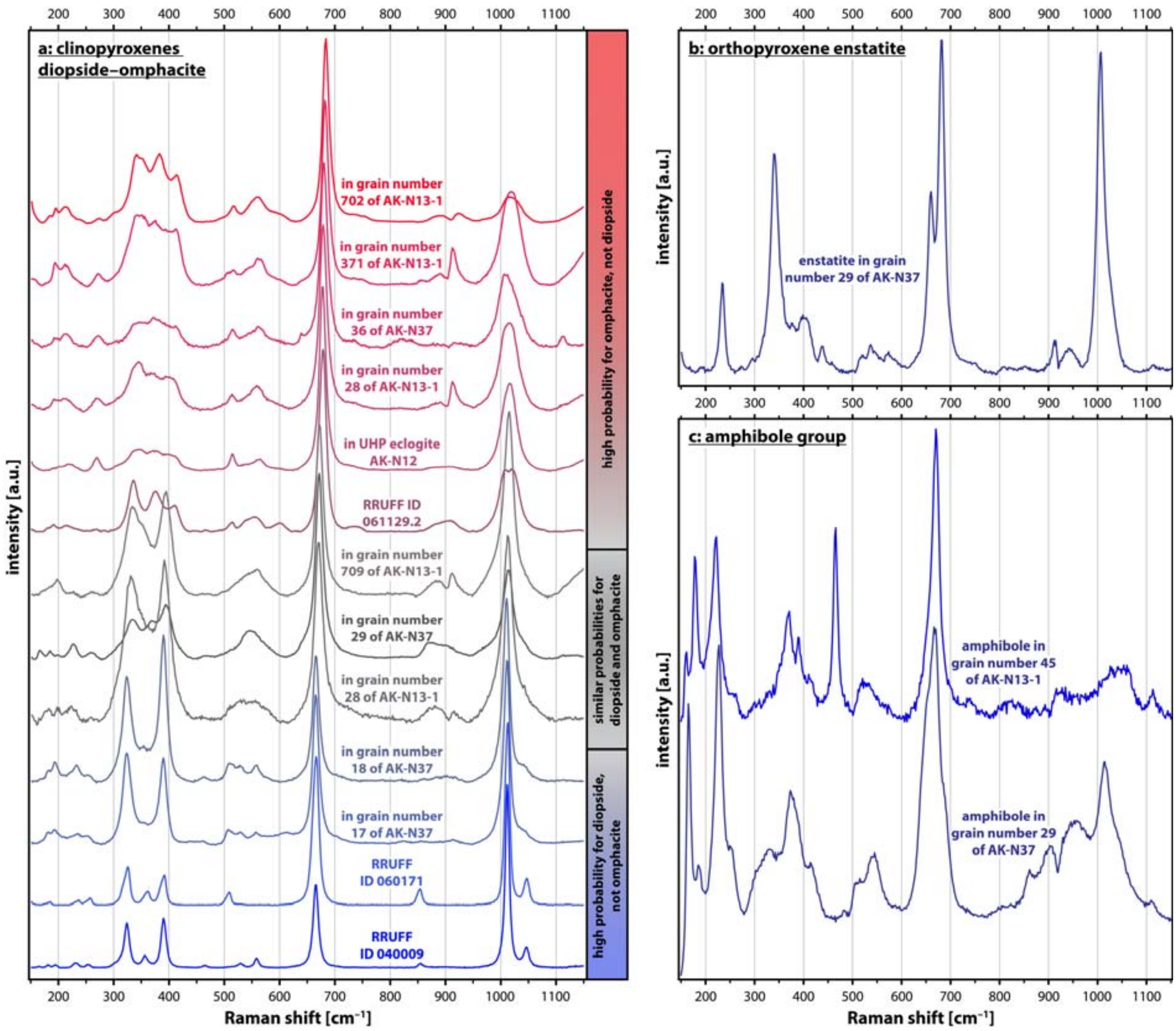
a: clinopyroxenes
diopside–omphacite
in grain number
702 of AK-N13-1
in grain number
371 of AK-N13-1
in grain number
36 of AK-N37
in grain number
28 of AK-N13-1
in UHP eclogite
AK-N12
RRUFF ID
061129.2
in grain number
709 of AK-N13-1
in grain number
29 of AK-N37
in grain number
28 of AK-N13-1
in grain number
18 of AK-N37
in grain number
17 of AK-N37
RRUFF
ID 060171
RRUFF
ID 040009
high probability for omphacite, not diopside
similar probabilities for diopside and omphacite
high probability for diopside, not omphacite
intensity [a.u.]
Raman shift [cm⁻¹]
b: orthopyroxene enstatite
enstatite in grain
number 29 of AK-N37
c: amphibole group
amphibole in
grain number 45
of AK-N13-1
amphibole in
grain number 29
of AK-N37

Fig. 5

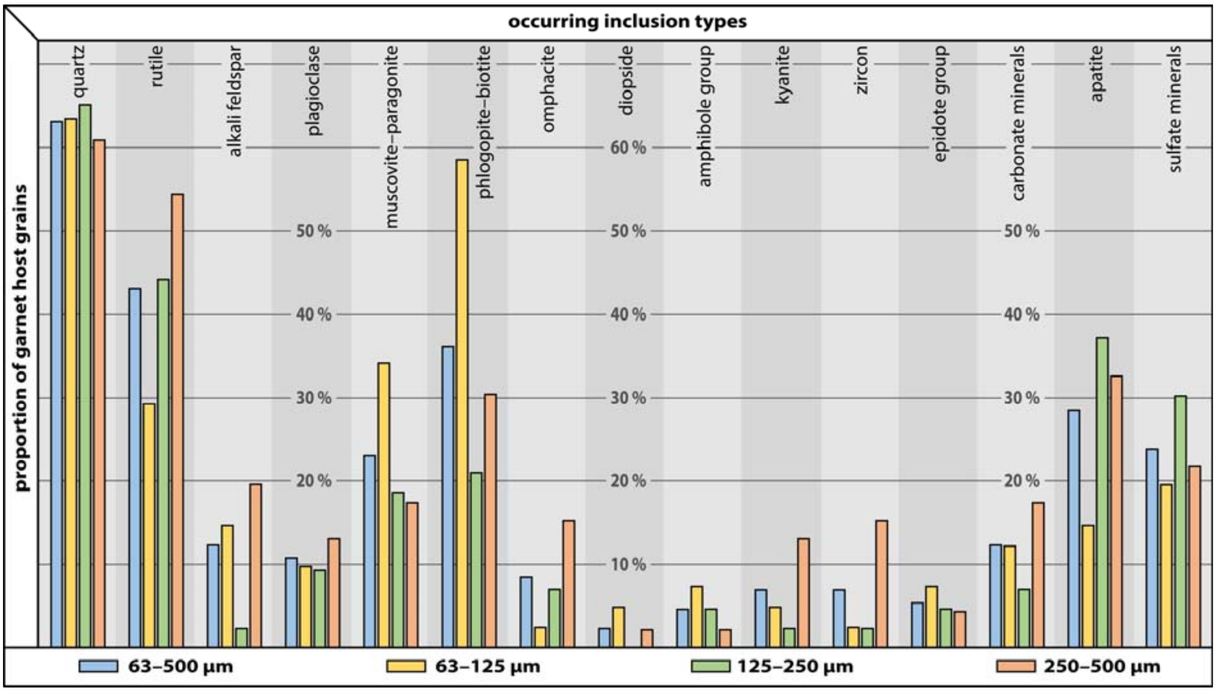
occurring inclusion types
proportion of garnet host grains
quartz
rutile
alkali feldspar
plagioclase
muscovite–paragonite
phlogopite–biotite
omphacite
diopside
amphibole group
kyanite
zircon
epidote group
carbonate minerals
apatite
sulfate minerals
60 %
50 %
40 %
30 %
20 %
10 %
63–500 µm
63–125 µm
125–250 µm
250–500 µm

Fig. 6

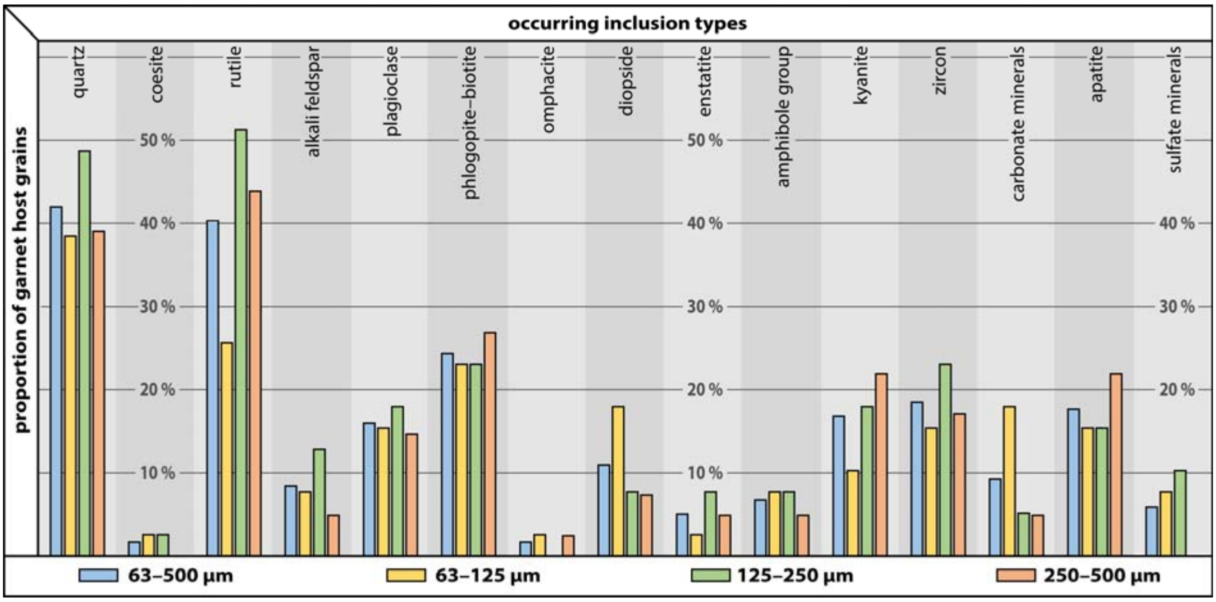
occurring inclusion types
quartz
coesite
rutile
alkali feldspar
plagioclase
phlogopite–biotite
omphacite
diopside
enstatite
amphibole group
kyanite
zircon
carbonate minerals
apatite
sulfate minerals
proportion of garnet host grains
50 %
40 %
30 %
20 %
10 %
63–500 µm
63–125 µm
125–250 µm
250–500 µm

Fig. 7

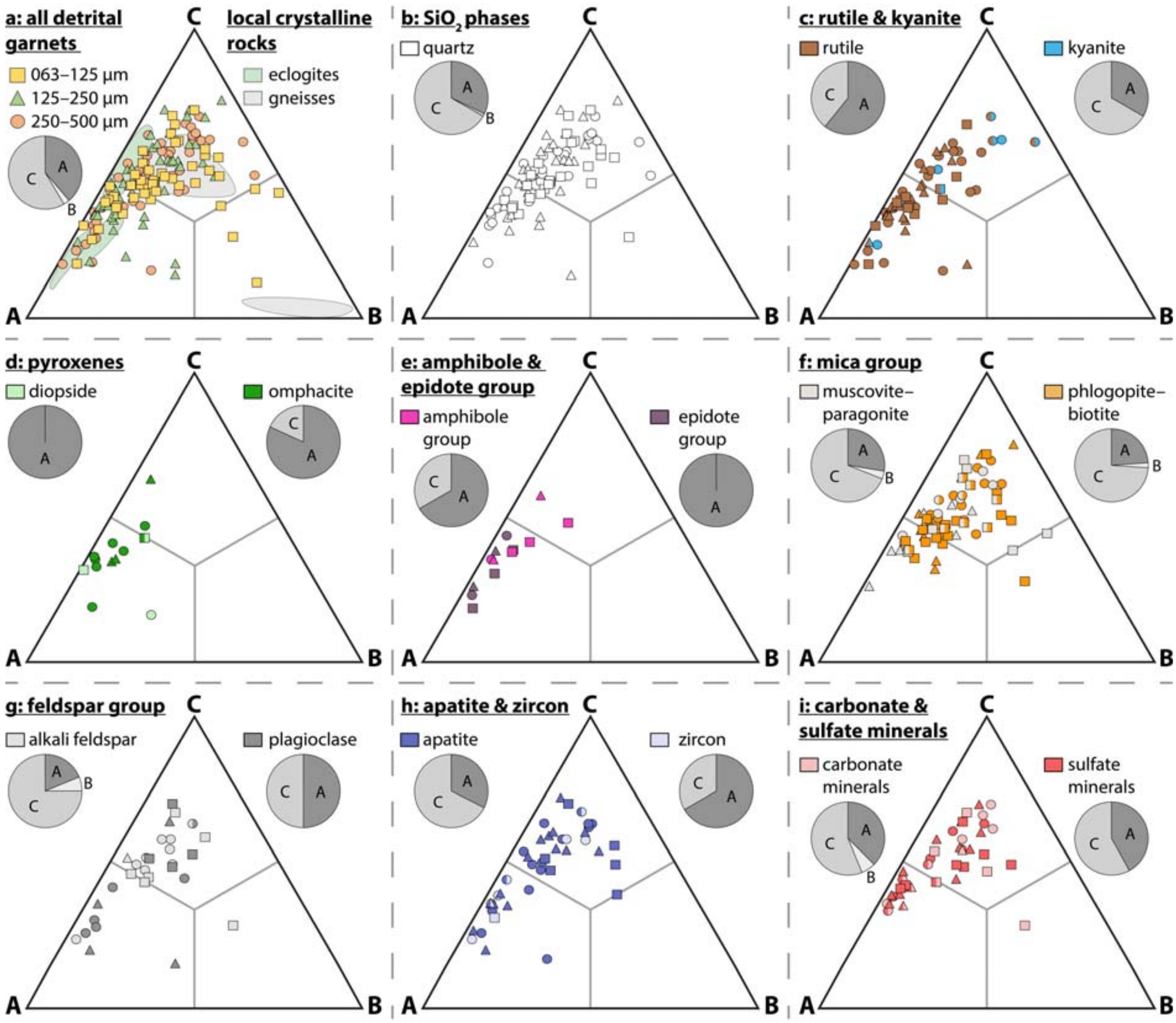
a: all detrital garnets
local crystalline rocks
063–125 µm
125–250 µm
250–500 µm
eclogites
gneisses
b: SiO2 phases
quartz
c: rutile & kyanite
rutile
kyanite
d: pyroxenes
diopside
omphacite
e: amphibole & epidote group
amphibole group
epidote group
f: mica group
muscovite–paragonite
phlogopite–biotite
g: feldspar group
alkali feldspar
plagioclase
h: apatite & zircon
apatite
zircon
i: carbonate & sulfate minerals
carbonate minerals
sulfate minerals
A
B
C

Fig. 8

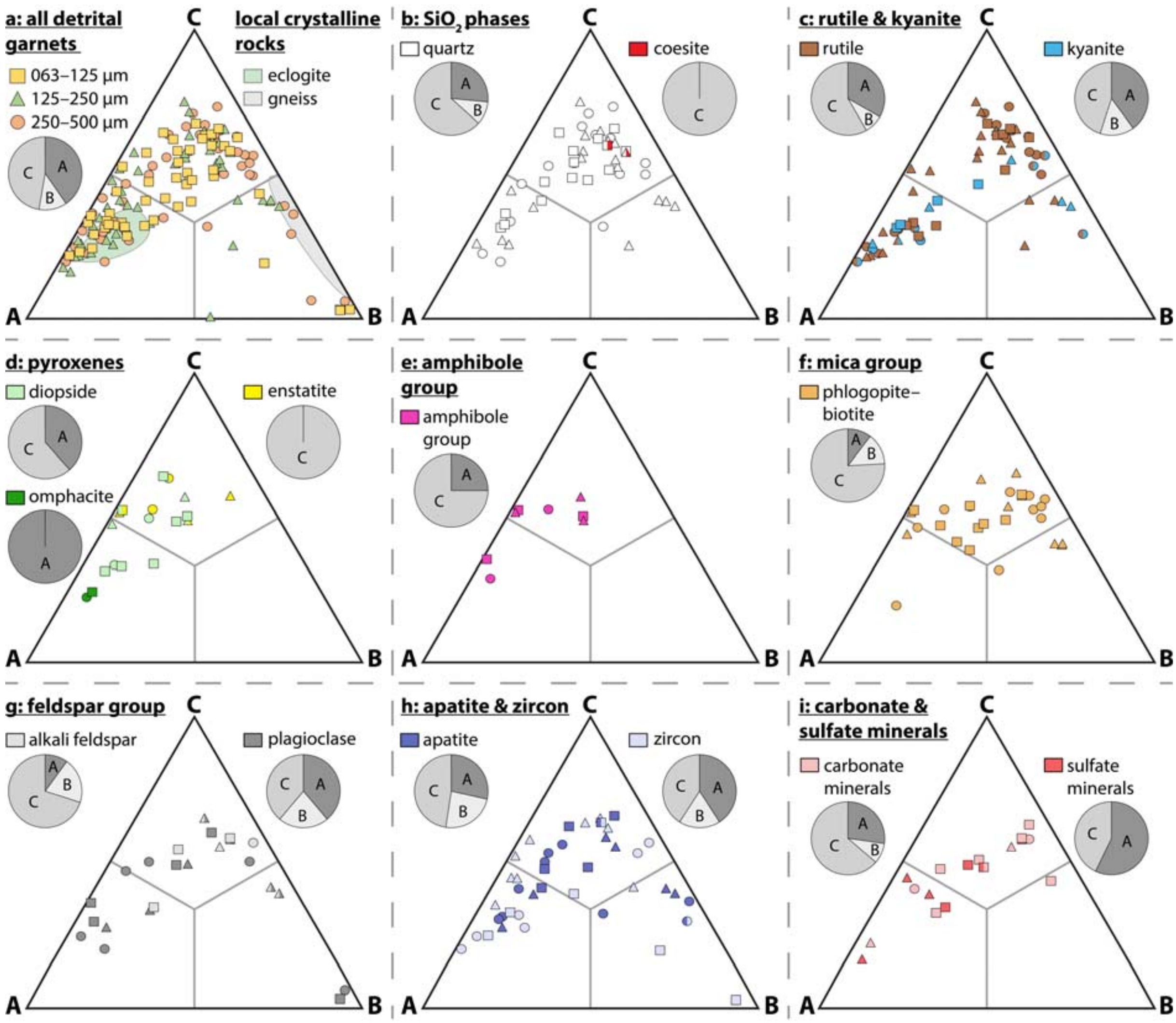

a: all detrital garnets
063–125 µm
125–250 µm
250–500 µm
local crystalline rocks
eclogite
gneiss
b: SiO2 phases
quartz
coesite
c: rutile & kyanite
rutile
kyanite
d: pyroxenes
diopside
enstatite
omphacite
e: amphibole group
amphibole group
f: mica group
phlogopite–biotite
g: feldspar group
alkali feldspar
plagioclase
h: apatite & zircon
apatite
zircon
i: carbonate & sulfate minerals
carbonate minerals
sulfate minerals
A
B
C

Fig. 9

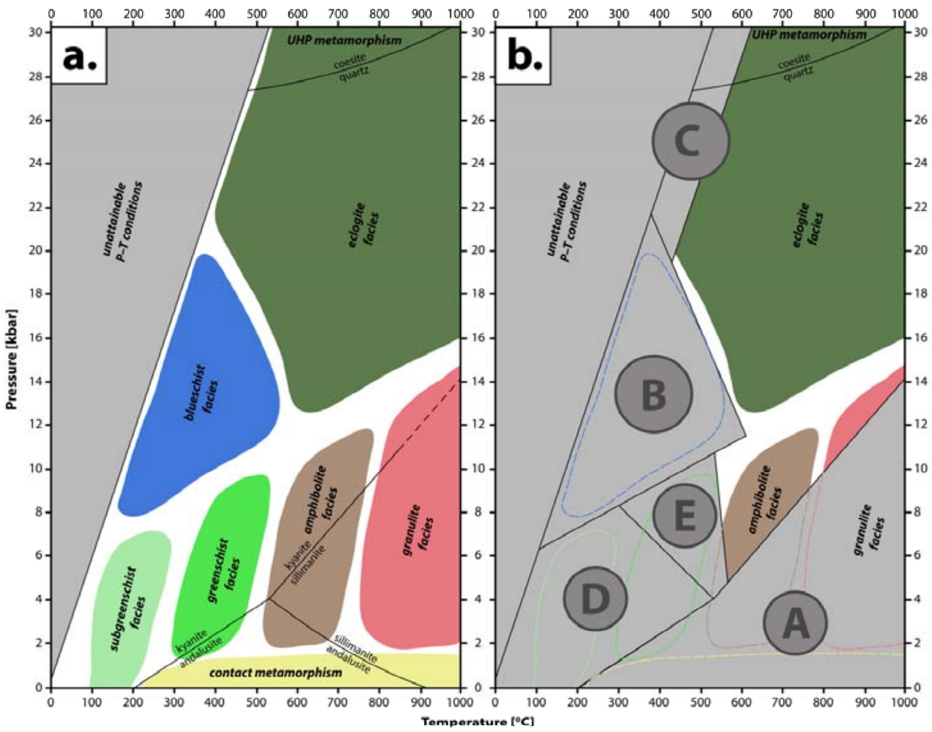
a.
b.
UHP metamorphism
coesite
quartz
unattainable P–T conditions
eclogite facies
blueschist facies
subgreenschist facies
greenschist facies
amphibolite facies
granulite facies
kyanite
sillimanite
andalusite
contact metamorphism
Pressure [kbar]
Temperature [°C]
A
B
C
D
E

Fig. 10

Table 1

	Rock types	Grt	Qz	Coe	Rt	Afs	Pl	Wmca	Phl–Bt	Omp	Aug	Opx	Amp	Ky	Ep	Cb
amphibolite facies	Micaceous Qz-Fsp-gneiss[1]	±	+	–	–	+	+	±	+	–	–	–	±	–	+	–
	Megacrystic felsic gneiss[1]	+	+	–	–	+	+	–	+	–	–	–	±	–	±	–
	Layered garnetiferous felsic gneiss[1]	+	+	–	–	+	+	±	+	–	–	–	+	–	+	–
	Layered garnetiferous felsic gneiss (mafic interlayers)[1]	+	–	–	–	+	+	–	+	–	–	–	+	–	–	–
granulite facies	Megacrystic felsic gneiss[1]	+	+	–	–	+	+	–	+	–	±	–	±	–	–	–
	Layered garnetiferous felsic gneiss[1]	+	+	–	–	±	+	–	+	–	±	–	–	±	–	–
	Layered garnetiferous felsic gneiss (mafic interlayers)[1]	+	–	–	–	–	+	–	–	–	+	–	–	–	–	–
	Mafic to intermediate dykes and pods[1]	+	±	–	–	±	+	–	±	–	+	–	–	–	–	–
	Dioritic to gabbroitic pods[1]	+	–	–	–	–	+	–	±	–	+	–	–	–	–	–
	Anorthositic pods[1]	+	±	–	–	±	+	–	±	–	+	±	–	–	–	–
eclogite facies	Layered garnetiferous felsic gneiss[1]	+	+	–	–	–	–	+	–	+	–	–	–	+	+	–
	Layered garnetiferous felsic gneiss (mafic interlayers)[1]	+	+	–	±	–	–	–	–	+	–	–	–	–	–	–
	Mafic to intermediate dykes and pods[1]	+	+	–	±	–	–	±	–	+	–	–	–	–	±	–
	Dioritic to gabbroitic pods[1]	+	+	–	–	–	–	–	+	+	–	–	–	–	+	–
	UHP eclogite AK-N12[2,3]	+	+	±	+	–	–	+	–	+	–	–	+	+	+	+
	UHP eclogite Straumen[4]	+	+	±	+	–	–	+	–	+	–	–	+	+	+	+

\+ always present /// ± rare /// – not present